Автономная некоммерческая образовательная организация высшего образования «Сколковский институт науки и технологий»

На правах рукописи

Ибаниес Федерико Мартин

МОДЕЛИРОВАНИЕ, УПРАВЛЕНИЕ И РЕАЛИЗАЦИЯ МНОГОПОРТОВЫХ ПРЕОБРАЗОВАТЕЛЕЙ И ИНВЕРТОРОВ ДЛЯ ИНТЕГРАЦИИ ЭЛЕКТРОМОБИЛЕЙ В ЭНЕРГОСЕТЬ

Специальность: 1.2.2. Математическое моделирование, численные методы и комплексы программ

АВТОРЕФЕРАТ
диссертации на соискание ученой степени доктора технических наук

Москва – 2025

Работа выполнена в Центре энергетических технологий Автономной некоммерческой образовательной организации высшего образования «Сколковский институт науки и технологий»

Научный консультант: (при наличии)	**Фамилия Имя Отчество, ученая степень, ученое звание (при наличии)**
Ведущая организация: (при наличии)	наименование организации

Защита состоится **число месяц год в 00 часов 00 минут** на заседании диссертационного совета **ШИФР СОВЕТА (при наличии)**, созданного на базе Автономной некоммерческой образовательной организации высшего образования «Сколковский институт науки и технологий» (Сколтех)

по адресу: Территория Инновационного Центра «Сколково», Большой бульвар д.30, стр.1, Москва 121205

С диссертацией можно ознакомиться в библиотеке Сколтеха и на сайте организации https://dissovet.skoltech.ru/

Автореферат разослан «___» _____ 2025 г.

Ученый секретарь диссертационного совета
ученая степень — Фамилия Имя Отчество

Autonomous Non-Profit Organization for Higher Education
"Skolkovo Institute of Science and Technology"

As a manuscript

IBANEZ FEDERICO MARTIN

MODELING, SIMULATION AND IMPLEMENTATION OF MULTI-PORT CONVERTERS AND INVERTERS FOR INTEGRATING ELECTRIC VEHICLES IN THE UTILITY GRID

Specialty: 1.2.2.Mathematical Modeling, Numerical Methods and Software

DISSERTATION ABSTRACT
of the dissertation for the Degree
of Doctor of Science in Engineering

Moscow - 2025

The work was performed at the Center of Energy Science and Technology of Skolkovo Institute of Science and Technology.

Scientific supervisor:	**Full Name, academic degree, academic title (if available)**
Consultant: (if applicable)	**Full Name, academic degree, academic title (if available)**
Leading organization: (if applicable)	**Name of the lead organization**

The defense will take place on **day month year time** at the meeting of the Dissertation Council **CIPHER of the COUNCIL (if available)**, based at Skolkovo Institute of Science and Technology (Skoltech)

address: Skolkovo Institute of Science and Technology, the territory of the Innovation Center “Skolkovo", Bolshoy Boulevard, 30, bld.1, Moscow 121205, Russia

The text of the dissertation is available at the Skoltech library or on the website https://dissovet.skoltech.ru/

Dissertation Abstract was sent on «___» _____ 2025.

Academic secretary of the Dissertation Council Full Name
academic degree of the Academic Secretary

GENERAL CHARACTERISTICS OF THE WORK

The relevance of the research topic is due to the increased demand on the electric grid associated with the increased number of electric vehicles in Russia and, in general, in the world. A fraction of fuel-based vehicles will be replaced by electric vehicles (EVs), which will draw power the electric grid. This will have an impact on the electric grid consumption and it will require new infrastructure investments. In order to smooth this transition, electric vehicles can be partially charged by local generation and storage. Thus, the grid does not need to supply all the power from the main power plants.

To implement this idea, local photovoltaic panels and batteries can be installed at the point of charging and use that energy to charge the vehicle when it is needed. Thus, multiple sources can simultaneously charge the EV through a power converter or a set of power converters. These converters must manage power flow from different sources, including the grid, batteries and photovoltaic panels.

In case of using a set of two-port converters, the converters will have a common DC link in one of their ports and the other port will be connected to the sources or loads. Thus, one converter will be connected to the grid, one converter will be connected to the internal batteries, one converter will be connected to the photovoltaic panels (PVs) and another one to the vehicle to be charged. Internally, all of them must be interconnected via a common DC link as shown in Figure 1(a). In this way, the system will need as many converters as the number of connected sources or loads. This solution is valid but it requires the coordination of multiple devices and an excess of components. A multi-port converter can perform the same functions but in a single circuit which is easier to manage. Figure 1(b) clarifies the idea of the multi-port converter and compares it with the alternative solution which consists of a set of two-port converters. Multi-port converters are a relatively new concept in which energy is delivered to multiple points at different voltage and current levels.

In addition, multi-port converters can also find other relevant applications such as uninterruptible power supplies (UPS), power electronic transformers (to connect different grids electronically with galvanic isolation), multiple output power supplies, (for example in aircrafts where many voltages are needed), and hybrid energy storage systems.

The degree of scientific development of the problem. Researchers worldwide have been actively studying multi-port converters. These converters are becoming relevant due to their ability of multidirectional power flow and galvanic isolation [1]. In general, multi-port converters include converters based on transformers and other impedance networks, such as resonant converters [2], multi-transformer converters [3], complex impedance networks [4-6] and single multi-winding transformer-based converters [7-8]. Converters based on transformer are attractive because of the implicit galvanic isolation between ports. High-frequency (kHz range) transformers allow galvanic isolation between ports, however, they should be carefully designed in order to keep parameters such as its magnetizing inductance and leakage inductances under design requirements [A23].

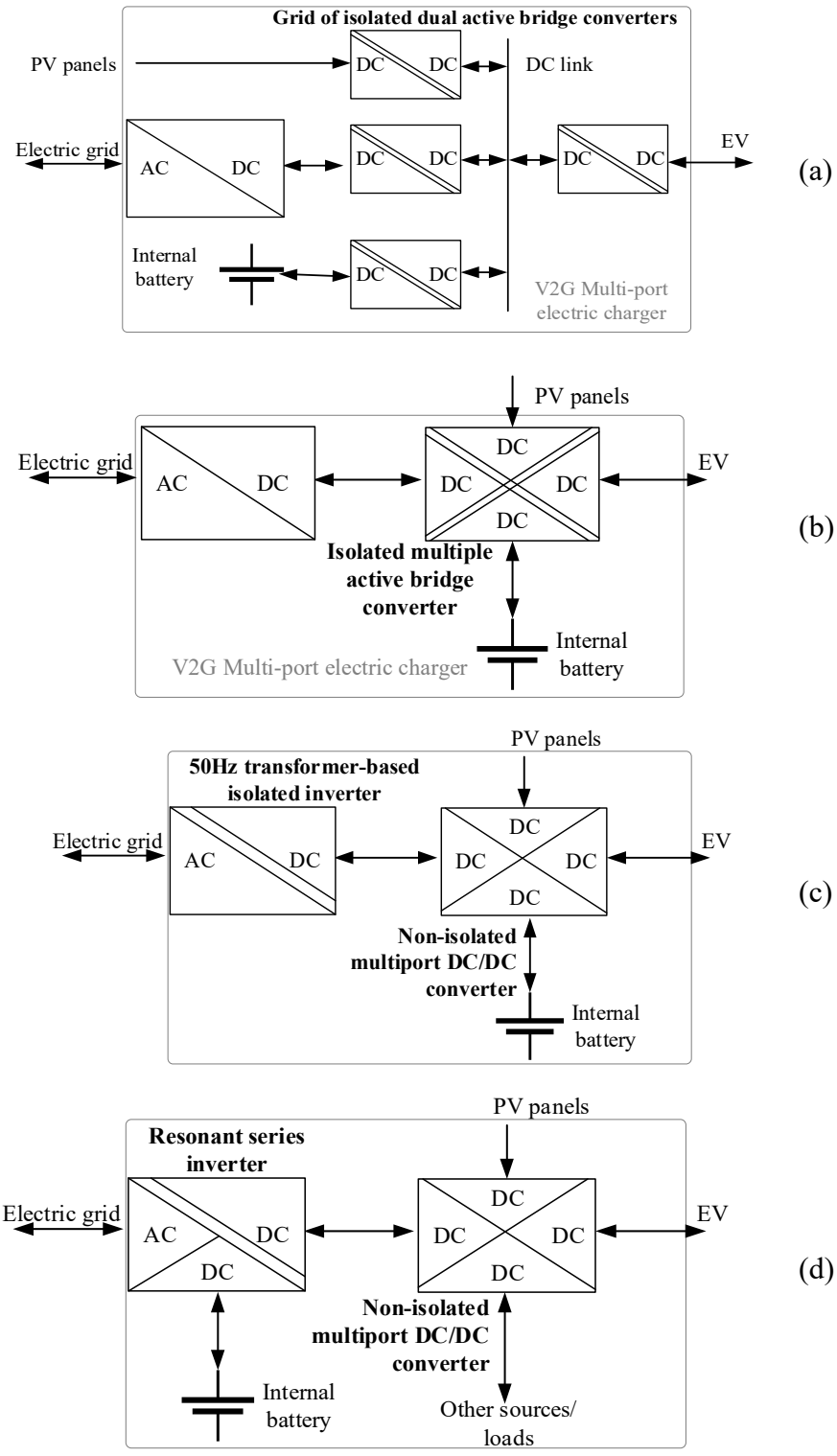

Figure. 1- Electric charger: (a) using 2-port converters and (b) using a MAB converter (c) partial isolation solution based on non-isolated converter (d) partial isolated resonant DC/AC

Among multi-port converters, multiple active bridge converters or MAB converters are particularly of interest due to the fact that they require the minimum number of passive elements and a moderate number of active elements such as

electronic switches (bipolar junction transistors, MOSFETs, IGBTs or others). A general MAB converter is shown in Figure 2, where each DC port is connected through a DC/AC bridge, which, in general, can be a half-bridge, a full-bridge, Neutral Point Clamped (NPC) DC/AC, T-type DC/AC and even three-phase configurations. Each solution for the bridge allows different number of output levels. A half-bridge allows 2 levels, a full-bridge allows 3 levels and the others more but require more components. Each type of bridge has its benefits and drawbacks. This research work is focused on MAB converters based on a single multi-port transformer connected to several full-bridge DC/AC stages. However, the same proposal can be applied to any other type of MAB converters. In Figure 2, the version of four ports is presented, however, the number of ports is arbitrary and depends on the application.

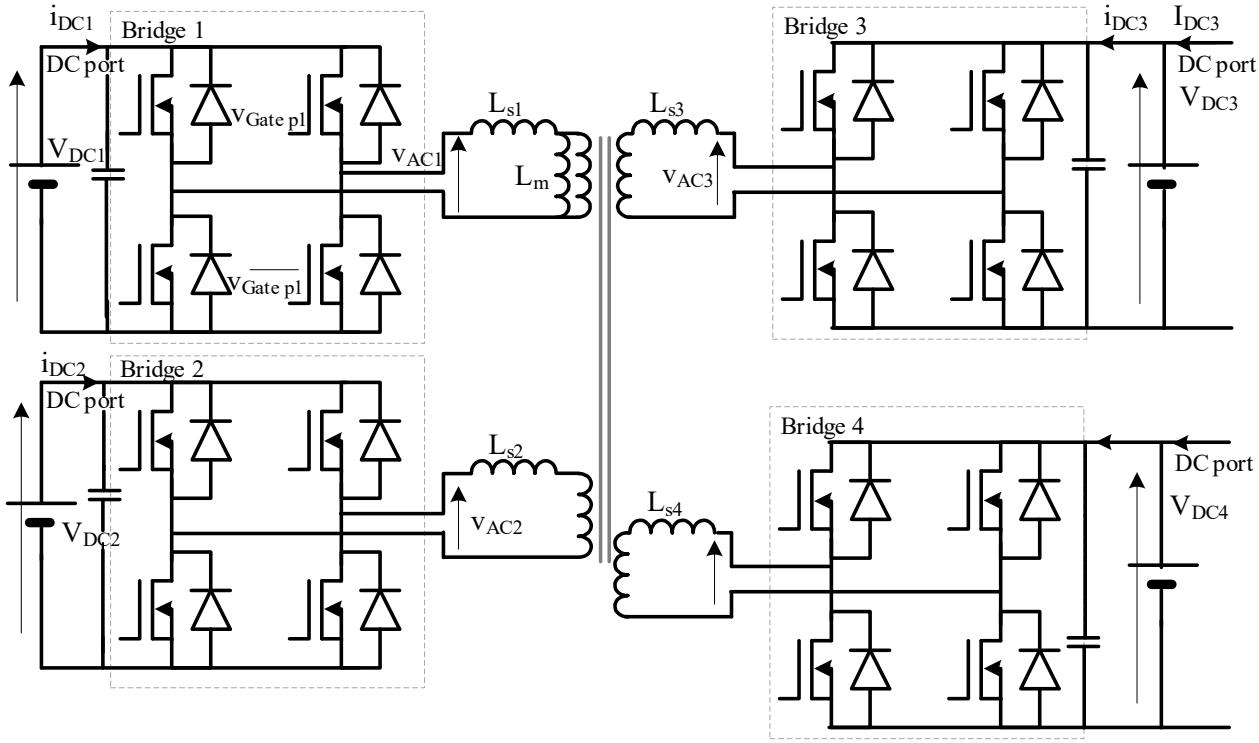

Figure. 2- Example of a MAB converter: QAB (quad-active bridge) power stage diagram, which can be easily extended to a larger number of ports

MAB converters can be seen as an extension of dual active bridge (DAB) converters [9] in terms of DC/AC bridges, the transformer as the element to transfer the energy and the modulation techniques. DAB converters are extremely useful in systems which need to be isolated from the grid, so the isolation can be performed using small-size high frequency transformers. The main method to transfer the energy from one port to the other one is based on a phase shift modulation between the two ports, also known as single-phase-shift (SPS) [9]. The technique is commonly used for transferring power in electric grids, where the phase difference between ports is a function of the amount of transferred power. This modulation works well if the voltages at each port are similar, however, if the voltage at the ports are able to vary, the efficiency droops drastically due to the excessive reactive power involved. This

happens typically for battery or supercapacitor charging/discharging processes, where the voltage is a function of the state of charge [10, 11].

The first MAB converter was the triple active bridge (TAB) converter introduced by Zhao, Kolar *et al* in 2004 [12-14]. It provides good efficiency, bidirectional power flow and galvanic isolation. The TAB suffers from coupling effects between ports, meaning that delivering power from port 1 to port 2 might have some power delivery to port 3. This coupling effect should be minimized by advanced control methods in which the phase modulation should be accurately selected in order to keep the power flow in the desired direction cancelling any non-desired direction.

For that reason, Zhao, Kolar et al. have proposed a decoupling method for TAB which allows to control the power in each port independently based on phase shift modulation [12]. The method is attractive but it has some limitations: it is difficult to extend it to a larger number of ports and it does not include the transformer dynamics. For increasing the number of ports, the control technique becomes too complex [13]. The phase shift modulation to control power transfer [14-15] is simple, but it has some drawbacks, such as recirculating currents which increase the losses particularly when DC voltages at the ports should vary. This structure and control method have been used in certain applications such as solid-state transformers [13, 16], multi-port DC/DC converters for medium voltage DC grids [17], aircraft [18] and electric vehicle chargers [19].

Recently, modern techniques were proposed to extend TAB converter's control to a larger number of ports and to minimize the DC current recirculation. The phase shift methods produce an excess of reactive power in the transformer which results in extra losses at low power transfer, thus, a phase shift with duty cycle modulation were proposed in [7, 20]. There, the duty cycle of each port is selected for increasing the efficiency [7]. However, this problem is non-linear and it is difficult for real-time calculations. Therefore, tables for selecting the proper duty cycles were obtained based on desired DC currents. However, as the number of ports increases, the table sizes increase considerably, so this method is hard to scale for a larger number of ports. Furthermore, this method neither includes the voltage dependence on DC ports nor the transformer dynamics.

Using Fourier decomposition allows to compute active and reactive power inside the converter (in the transformer ports) [21, 22] and this can be used to select the proper duty cycles. Resonant techniques were also explored in [2], however these techniques are too complex to extend them to a large number of ports.

Related to transients and dynamic performance of the MAB converter, authors from [7] claim that the transformer dynamics are always at a frequency close to the switching frequency, so they can be neglected. However, to have good efficiency and control of the power flow using phase shift, the reactance-resistance ratio (X/R) in each port should be large. As the ratio increases, the winding time-constant increases as well. Thus, the transformer dynamics can affect the plant and must be taken into account, otherwise the control bandwidth should be limited. This aspect was not explored yet, and it is one of the novelties of the presented work. The research work

will allow the multiple active bridge converter to work with variable DC sources. This includes bidirectional flow in every port and an improvement in efficiency.

As the MAB is a DC/DC converter, so all of its ports are DC ports. Therefore, for connecting it to the electric AC grid an inverter must be added, the complete EV charger is shown in Figure 1(a). There are many inverter topologies that can do that connection successfully, such as voltage source inverters (VSI) [23], current sources [24] inverters, impedance source inverters [A8] multi-level inverters and others [25]. For low voltage AC grids (three-phase 230V-50Hz), VSI are preferred due to the minimal number of components. It consists of a three-leg bridge of switches and a passive filter with no isolation.

As the EV charger proposed in Figure 1(b) has an isolated multiple port converter, the inverter does not require additional galvanic isolation, which makes the VSI a good choice due to its compactness. The control technique of VSI is an actual topic because it allows to perform many services to the grid. VSIs can work in any mode by absorbing or delivering active or reactive power. So, they can be used for controlling the voltage of the grid at a certain grid node by injecting reactive power, or for example, they can assist the frequency regulation by transferring active power [28]. They can also emulate variable passive elements such as capacitors or inductors to improve the grid quality and they can work as an active filter for reducing the harmonic components in the grid [29]. For the case of the EV charger, due to the extensive possibilities of the inverter control methods and the bidirectional power flow feature of the MAB converter, the EV charger can deliver or absorb energy to/from the grid, performing grid-to-vehicle (G2V) and vehicle-to-grid (V2G) modes. In the absorbing mode, it is clear that it will charge the EV battery and it will work as a rectifier to provide a DC voltage to the MAB converter. However, in V2G mode, the inverter can work as a slave by delivering power according to a reference or can work as a grid-forming inverter.

Grid-forming inverters are one of the current topics in inverter control. Inverters can control the grid by regulating the voltage delivering the necessary power to the loads. However, if the consumption is higher than the inverter power capacity, more than one inverter should be connected and they need to share the load. For that, several modern techniques have been developed, particularly the droop control method, a decentralized approach that enables load sharing among inverters. While droop control facilitates power sharing, transient conditions can lead to power oscillations and high voltages/high currents spikes [30].

For mitigating such oscillations, this research work includes the modeling of a weak grid based on inverters. From that, guidelines for a proper control were extracted. In addition, to limit high currents during transients, new protections have been proposed which includes virtual impedance, phase limiters and power filters.

The solution of a MAB converter with an inverter is not the only alternative to Figure 1(a). This depends on the characteristics of each DC ports in terms of isolation. Partial isolated systems can be an alternative to Figure 1(a) and (b). This research work also suggests new topologies of EV chargers: in Figure 1(c), a combination of a non-isolated multiple port converter and inverter with an isolation transformer, and, in Figure 1(d) a resonant DC//DC/AC converter which has one isolated DC port.

Resonant converters have been studied for several years. They are attractive due to their high efficiency but their control becomes complicated for variable loads. Most common resonant converters are series, parallel and LLC converters [31]. Usually these converters work in only one power flow direction but they can be extended to bidirectional applications with some modifications. The author has introduced novel techniques for obtaining a bidirectional series resonant converter for energy storage applications in [A7, A9-A14]. Based on that, in this work a series resonant inverter with one isolated and one non-isolated DC ports is proposed as a compact solution for EV charger.

The **goal** of the study is to model, simulate and implement a system based on power electronic converters capable of sharing energy between its multiple ports with high efficiency and ease of implementation. Most ports are ports are "DC type" such as DC sources (batteries, supercapacitors, fuel cells, photovoltaic panels) or loads and at least one port is an "AC type" due to the grid connection possibility. The system or **object** should be able to manage a large number of ports with bidirectional power flow; thus, a control algorithm must be designed. In the case of "AC type" grid connection should be allowed.

For achieving this goal, it requires to **address the following research problems**:

- To identify the main issues by studying the existing control methods.
- To make a mathematical model of a multiple active bridge converter.
- To propose a control method that can consider variable voltage DC sources in the converter's DC ports.
- To implement the control method for conducting experiments.
- To evaluate the method by means of computer simulation of mathematical models and real experiments.
- To compare the different proposed techniques and highlight their benefits and drawbacks.
- To make a mathematical model of a grid-connected inverter.
- To propose a new control method for parallel inverters in the grid for sharing power with smooth transients.
- To suggest an alternative to the MAB converter with the inverter considering partial isolation using non-isolated converters
- To suggest an alternative to the MAB converter with the inverter considering partial isolation using resonant techniques for having at least one isolated port.

The scientific novelties which are also **the main results submitted for the defense** are:

1. A new mathematical model for describing the multiple active bridge converter based on a rotational frame synchronized with the main operational frequency.
2. A decoupling control method that allows the use of any number of ports in a multiple active bridge converter and allows to transfer energy from any port to any other port without sending power to any third port. The proposed

decoupling method allows to control the active power between ports and also the amount of reactive power in each transformer's winding.

3. Efficiency improvements for multiple active bridge converters. The control method considers the effect of the voltage change in the DC ports which are compensated internally by the modulation technique. Thus, efficiency is higher in comparison with other control methods (single phase shift method) in the condition of non-equal voltage at the DC ports. Also, a new specific modulation called "dual duty" was proposed and implemented in order to reduce even more the conduction losses and increase efficiency for delivering power among ports.
4. As a grid-connected inverter is also required to integrate the proposed DC/DC converter to grid applications, modeling of grid inverters in weak and strong grids was developed. Based on this modeling, improvements in connection transients of grid-forming inverters by means of introduction of phase limiters, controllable virtual impedance and power filters were achieved.
5. The controller of the inverter should tolerate changes in the grid, thus, an adaptive controller was proposed which controls the output current of the inverter and compensated the possible harmonics.
6. As an alternative to the MAB converter with inverter, when complete isolation is not needed (only one of the ports needs to be isolated), the design, modeling, simulation and testing of two new more compact solutions were performed: a non-isolated high-gain DC/DC/DC converter with reduced number of components, and a multiple port power converter with one isolated DC port and other AC and DC ports (DC//DC/AC) avoiding the inverter.

The theoretical and practical significance of the research. The main conclusions of the dissertation research can be used for developing real fast electric vehicle chargers with the possibility to reduce the peak power consumption of the grid. The results of the research work include new models and control algorithms for multi-port systems which allow the connection of multiple AC or DC sources in a system where the power flow can be totally controlled. Many applications can take advantages of this new methods. The research work proposes a circuit that improves fast EV chargers with local generation and storage for reducing the grid peak power demand. This has a direct practical application and can be implemented massively in the electric grid. For that reason, a patent was published in 2024.

Furthermore, the same system can also be used for other multiple port systems such as uninterruptible power supplies (UPS), electronic transformers, hybrid energy storage systems, interconnection with multiple voltage grids such as in aircrafts and other vehicles, smart houses and others.

The **methodology** is based on analyzing multi-port systems, particularly multiple active bridge (MAB) DC/DC converters. The research is based on other traditional converter analysis such as dual active bridge (DAB) converter and triple active bridge (TAB) converters proposed by Prof. Kolar and Prof. Zhao The research involved modeling, control techniques, electronic circuit design, and coding. The research was validated through numerical simulations and laboratory experiments, including

prototype development and testing with using high-quality measurement instruments and bidirectional power sources to emulate the different elements of the system and its applications.

The **validity and reliability of the results and conclusions** were confirmed by numerical simulation and experimental validation with accurate electronic instruments such as digital oscilloscopes, current and differential voltage probes, laboratory power supplies, impedance analyzers, and prototypes developed in the laboratories of Skolkovo Institute of Science and Technology. The reproducibility of the results was confirmed by repeating experiments three times and comparing them with numerical simulations. The statements and conclusions formulated in the dissertation have been approved by the committees of experts in international scientific conferences. The credibility is also confirmed by the publications of research results in peer-reviewed scientific journals.

The **personal contribution of the author** includes three main parts: inverters, multi-port DC/DC converters, and resonant converters. In terms of inverters, the proposition of new control techniques for inverters related to power sharing, protection and transients, particularly advanced droop control methods, virtual impedance, phase limiter and low-bandwidth communication for achieving power sharing and soft transients. For that, the modeling of inverters and implementation of the techniques in simulations and real inverters were performed. In multi-port DC/DC converters, the author has proposed a new modeling of the converter in dq-frame and due to that a novel control algorithm. The author modeled, simulated, and experimentally validated the system. Finally, in resonant converters, the author also proposed new ideas to reduce the size of converters in terms of number of switches. For that, intensive modeling and simulation was performed and finally validated through experiments.

Approbation of the work. 27 papers reflecting the main provisions of the study were published on the research topic, including 13 proceedings in international conferences with a total volume of 5 printer sheets, 14 publications in journals and collections of scientific papers with a total volume of 11 printer sheets. In addition, 1 patent in the Russian Federation was granted due to the invention in 2024. The list of papers is in the Section “Publications of the Author” at the end of the dissertation.

The research results were presented at international conferences in: IEEE PowerTech (Belgrade, Servia, 2023), IEEE APEC (Orlando, USA, 2023), IEEE IECON (Brussels, Belgium, 2022), IEEE ICRERA (Istanbul, Turkey, 2022), IEEE Industry Applications Society Annual Meeting (Vancouver, Canada, 2021), IEEE PES General Meeting Washington, DC, USA), IEEE PowerTech (Milan, Italy, 2019), IEEE PEDG (Xi'an, China, 2019). The main results of the dissertation research are also presented in the Electromobility course in the energy system master program of Skolkovo Institute of Science and Technology.

The structure and content of the work are determined by the conceptual ideas, which reflect the goal and objectives of the research. The dissertation consists of an introduction, 4 chapters, conclusion, and a list of 233 references. The main text of the work is presented on 384 pages, including 23 tables, 171 figures.

MAIN CONTENT OF THE WORK

Chapter 1 "Understanding the need of fast chargers and the impact to the grid". It is a brief introduction of the terminology related to fast chargers and their impact in the electric grid. It clearly indicates the reason of new solutions for fast chargers and, in general, multi-port systems. In addition, it shows other applications where multi-port converters can be used.

The Russian Federation and many other countries have decided to give a significant boost to the internal electric vehicle market with several programs that will increase both production and usage of electric vehicles (EV). Due to that, the increase of EV chargers will grow considerably and the utility grid will be heavily affected where a scenario of a much higher consumption will eventually appear. Thus, technologies that can reduce that impact of EVs and their chargers in the electric grid are of great relevance.

EV chargers are devices that connect the EVs to the grid and together they act as a new type of load. EV chargers are mainly divided in two big groups domestic chargers and public chargers. The first one is exclusively for the use of the vehicle owner and is often used at night from low to moderate power consumption. Public chargers on the contrary are installed in shopping malls, business centers and different parking places for charging EVs in a short amount of time at high power. As an example, a Tesla Model S requires around 5 hours to charge the vehicle for 100 km autonomy in a Mode 1 (AC single-phase 4 kW) charger, while it takes 22 minutes if a 50 kW mode 4 DC charger is used. Thus, those fast chargers are attractive from the point of view of the end-user (driver) but they can increase dramatically the grid consumption. Therefore, solutions that still allow the end-user high available power while demanding lower power from the grid are of great relevance. Otherwise, the grid infrastructure should tolerate those high-power peaks while EVs are being charged.

Regarding the technology, two types of chargers are mentioned: AC and DC chargers. An AC charger delivers AC (single- or three-phase connection) to the vehicle and there is an “on-board” charger which transforms the energy from the grid to the suitable values for the batteries in terms of voltage, current and waveform. In other words, there is an AC/DC circuit which controls the charging current inside the vehicle. Thus, those AC chargers are mainly a protection system with measuring features in order to understand the amount of energy delivered to the vehicle.

DC chargers are much more complex. DC chargers are directly connected to the EV battery. They do not use any “on-board” charger, the electronic circuits are inside the DC charger and this is why, it is possible to increase the transferred power. The standards suggest up to 80 kW, but companies have reached up to 1000 kW using different improvements such as water-cooled cables and other thermal technologies.

DC chargers require to convert three-phase AC power to the battery DC levels with galvanic isolation, so the vehicle is not in contact with the grid. For that, different types of electronic circuits have been proposed. The main issue is that in any case the energy should be extracted from the grid and delivered to the EV and this produces high demand in short time intervals which can overload the grid infrastructure. A

possible solution is to have in the charging point and additional energy source which can contribute to the charging process. This can be an in-site extra battery, photovoltaic panels or any other source of energy. This new architecture mitigates the high consumption in the grid, however, it requires a multiple port system which should be able to share the EV load among different sources. The following chapter will introduce the mentioned multiple port systems in their current state.

Chapter 2 " The multiple active bridge as a solution for a multi-port system." This chapter is divided in four sections. The first one reviews and studies the existing solutions to create a multi-port system for exchanging energy. It starts with simple integration of two-port systems to obtain a multi-port system and after that, it introduces the multiple active bridge as a promising solution. It mentions the main benefits and the main challenges. Based on that the research gaps are identified and the solutions are proposed. The 2nd section is focused on the multiple active bridge converter, its modeling and its control algorithms. It explains in details the novelty of the proposed control method. It describes the mathematical model and a control algorithm based on it for interpreting the behavior of a multiple active bridge converter. It explains the algorithms for inner and outer control loops and the main benefits regarding new degree of freedom in control references. The section also includes numerical simulation and the implementation in a real experiment at 1kW.

The 3rd section is focused on the effects of the delay times between the signals and their measurements. The control loops are affected and this section models this effect and proposes a solution to mitigate that. The last section is a comprehensive analysis of the power losses. It is presented based on mathematical models and computational simulations. Due to that, the section adds an original modulation technique that can reduce the conduction losses of the converter and increase efficiency by minimizing the root-mean-square currents through the transformer's windings. The implementation of this special modulation techniques in the form of pseudo-code for conducting computer simulations and real experiments are detailed. The section concludes with the benefits and challenges of the dual-duty modulation in comparison with other techniques.

Existing solutions for multiple port systems. A multiple port system can be realized in several ways. A first solution for a multiple port system is a combination of two-port DC/DC converters with one common DC link. Then, the ports which need single-phase or three-phase AC connection must be connected through an additional bidirectional DC/AC converter in order to have the required power signal. Figure 1(a) shows the solution.

A more compact solution is based on a multiple port converter in which several DC ports are interconnected [1-8]. A good candidate from these family of converters is the multiple active bridge (MAB) converter, which provides controllable bidirectional power flow, electrical isolation and compactness. Figure 1 shows the (a) common and the (b) MAB approaches. The MAB converter can be easily applied to other applications such as uninterruptible power supplies with PV panels, domestic

energy storage systems with multiple DC loads, hybrid energy storages and other multiple source systems.

MAB converters are becoming important due to their ability of multidirectional power flow and galvanic isolation. In general, MAB converters are part of a family of converters based on transformers [1] and other impedance networks, such as resonant converters [2], multi-transformer converters [3], complex impedance networks [4-6] and single multi-winding transformer-based converters [7-8]. One of the key elements of the MAB converter is the high-frequency (kHz range) transformer, which allows the isolation between ports, however, they should be carefully designed in order to keep parameters such as its magnetizing inductance and leakage inductances under design requirements [A23]. A basic diagram of a MAB converter is shown in Figure 2, where each DC port is connected through a full-bridge (but it can be any other topology).

MAB converters can be seen as an extension of dual active bridge (DAB) converters in terms of ports. The transformer, its leakage inductances and the modulation techniques are the key elements to transfer power between the ports. DAB converters are extremely useful in systems which need to be isolated from the grid, so the isolation can be performed using small-size high-frequency transformers. The main method to transfer the energy from one port to the other one is based on a phase- shift modulation between the two ports, also known as single-phase-shift (SPS) [9]. This technique is commonly used to transfer power in electric grids, where the phase difference between ports is a function of the amount of transferred power. SPS modulation works well if the voltages of each port are similar, however, if the port voltages are able to vary, the efficiency droops drastically due to the excessive reactive power involved. This happens typically for battery or supercapacitor charging/discharging processes, where the voltage is a function of the state of charge [10, 11].

For that reason, some advanced modulation techniques have appeared for DAB converters, such as the extended-phase-shift (EPS), double-phase-shift (DPS) and triple-phase-shift (TPS) modulations, in which the voltages at the transformer's windings are controlled through pulse width modulation to build three-level AC signals. In this way, the converter has more degrees of freedom to guarantee the power transfer with high efficiency, extending the zero-voltage-switching (ZVS) operation range of the converter and minimizing the reactive power and thus the current stress of the semiconductor devices.

In the case of MAB converters, the development was similar. In 2004, Prof. Zhao *et al.* introduced the first MAB in which the main control consisted of a phase-shift modulation with some initial ideas of duty modulation [12-14]. In 2007, J. Duarte *et al.*, proposed a phase-shift modulation for controlling hybrid fuel cells [15]. In 2008, Tao *et al.* incorporated duty modulation in order to reduce the switching losses. Unfortunately, the control algorithm is complex because there is a coupling behavior between ports. This means that delivering power from one port to another one might affect a third port if the control is not aware of that. In 2017, a different approach was introduced by Vermulst, Duarte *et al.* The method, based on Fourier series, is extremely complex because it extracts the Fourier components of the currents and controls them

at the switching frequency. In addition, the acquisition of the Fourier components can be noisy and can drag significant error [21, 22].

In 2022, a recent approach based on "perturb & observe" technique was introduced by O. M. Hebala *et al.* to look for the minimum RMS currents that guarantee the desired power flow [21]. The method is computational effective but it is slow due to the perturb and observe strategy. S. Bandyopadhyay *et al* have been used a linear active disturbance rejection controller to decouple the ports as well [26]. In 2024, another solution by Y. Cai *et al.* was to create virtual DABs inside the MAB and control them individually, the method uses Newton iterative algorithm in each control update [27]. It works for three ports but it becomes too complex for larger amount of ports.

As mentioned, a Fourier decomposition method was used to evaluate and minimize the losses by Vermulst, Duarte *et al.*and others [22]. The approach is interesting, however, obtaining high-frequency harmonics in a noisy environment is difficult. Due to that, in this research work, I have proposed to obtain the fundamental harmonic by hardware, and to use a real-imaginary decomposition to control the active and reactive power of each port independently. In this approach, both types of power are well controlled, so a desired amount of reactive power can be added to the active power to increase the phase-shift between current and voltage and to achieve soft-switching (ZVS) in the full bridges.

The dq-control method proposed in this thesis presents great efficiency for variable voltages at the DC ports and ease of control due to its fast response and decoupling capabilities. The next section details the method which can be used in MAB converters with a large number of ports. It starts with the development of a mathematical model of a MAB converter in a dq-frame representation. After that, a control algorithm is proposed, which is implemented in the form of block diagram. Using the model and the algorithm computer simulations were performed to evaluate the control algorithm. This includes the comprehensive study of harmonic problems and decoupling effects. The simulations were compared with real experiments where the control algorithms were implemented in c-code.

Mathematical modeling of a MAB converter using dq-frame representation. The MAB converter basic circuit, shown in Figure 2, consists of an AC circuit and multiple AC/DC or full-bridges so all of the output ports are DC ports. The AC/DC bridges have two ports, the DC port (or external ports) and the AC port or internal ports. The AC circuit can be considered as a $\mathbb{C}^{NxN}$ impedance matrix as shown in Figure 3(a), where N is the total number of ports [A2].

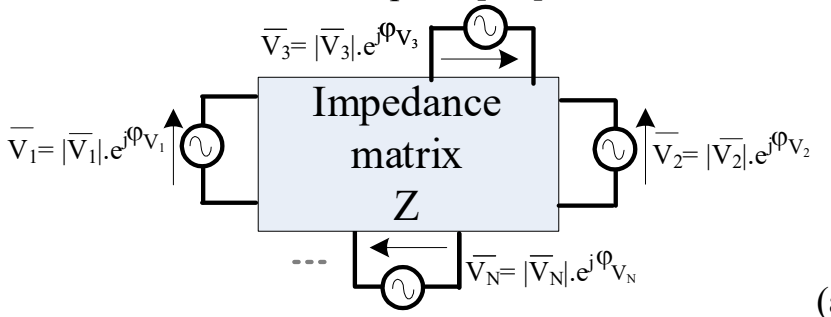

(a)

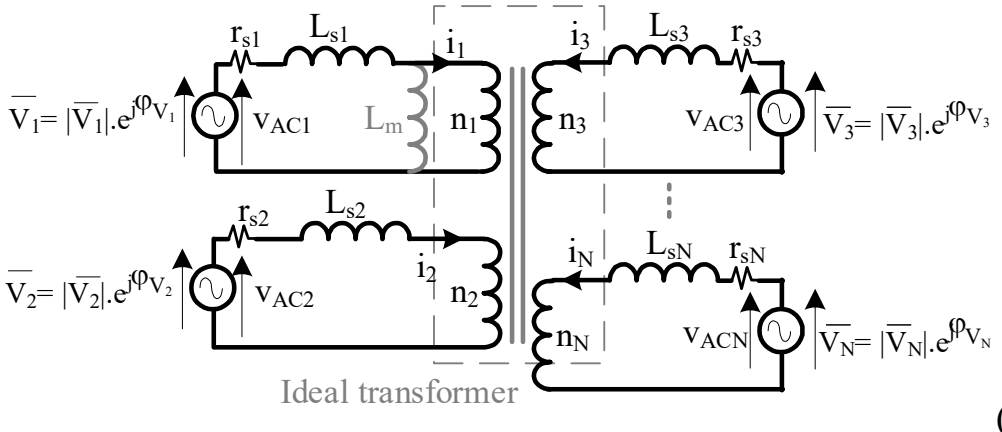

(b)

Figure 3- Example of MAB: (a) AC simplified diagram and (b) transformer model

Each DC port has an interface, an AC/DC bridge, which transforms the DC power into the AC signals according to pulse width modulation (PWM). Particularly, the full-bridge topology can set three voltage levels in the AC port: $+V_{DC}$, $-V_{DC}$ and 0V, as Figure 2 shows. The proposed modulation technique considers that the control will be performed on the fundamental harmonic ($\omega_0 = \omega_s = 1/T_s$ the switching frequency) of each AC port. The voltage signal in n-th AC port is:

$$v_n(t) = \underbrace{Im\left(\bar{V}_n . e^{j\omega_0 t}\right)}_{fully\ controllable} + \underbrace{Im\left(\sum_{p=2}^{\infty} \bar{V}_{np} . e^{jp\omega_0 t}\right)}_{non-controllable\ perturbation}. \quad (1)$$

It is a combination of a sine wave controllable in phase and amplitude and its non-controllable harmonics. Figure 4(a) shows an example of the modulation and its 1st harmonic component.

It is assumed that the power of the harmonics will be smaller than the fundamental. Thus, they will produce a power flow that can be considered as a perturbation at the AC power and it will be compensated using a DC power control loop as it is explained below in this chapter. In other words, the first harmonic approximation (FHA) is considered for the analysis and used in an inner (fastest) current control loop.

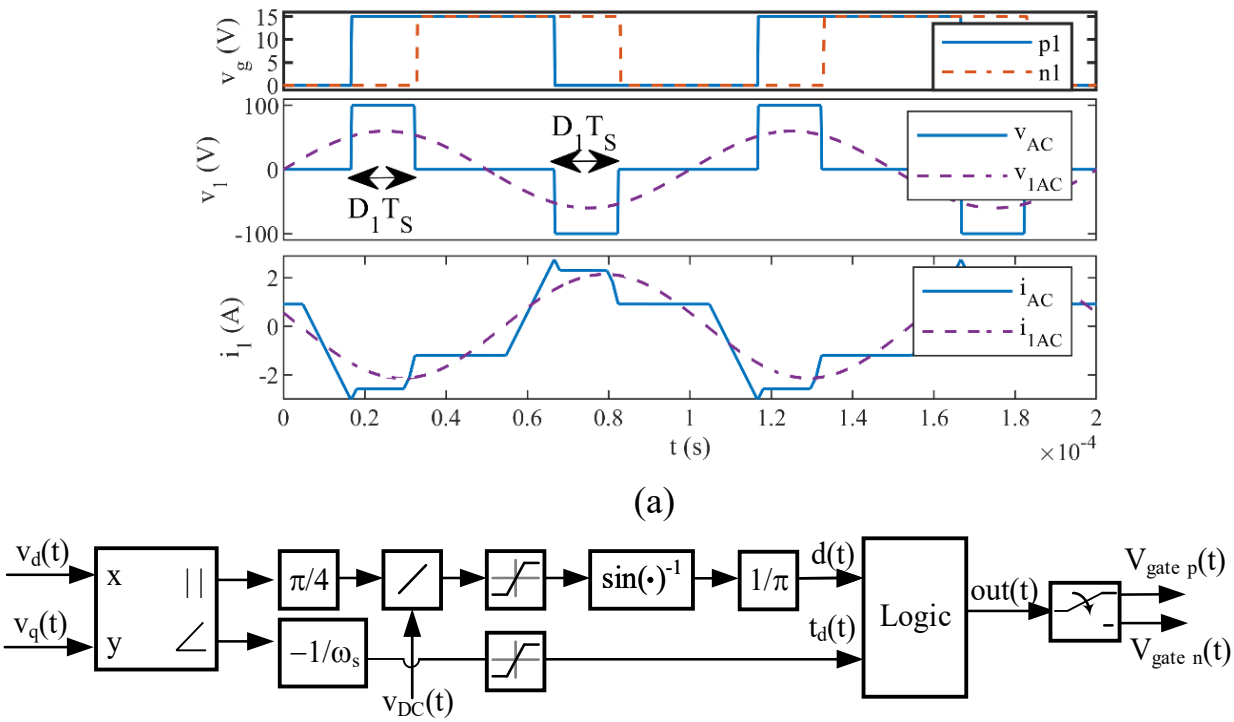

Figure 4- Single bridge diagram: (a) waveforms, (b) control logic diagram

The amplitude and phase of the n-th port 1st harmonic signal is a function of the duty cycle of the PWM signals:

$$|\bar{V}_n| = \frac{4}{\pi} V_{DCn}.\sin(D_n\pi)\ and\ \angle \bar{V}_n = \varphi_n, \tag{2.a}$$

and for its k-th harmonics:

$$|\bar{V}_{nk}| = \frac{4}{\pi k} V_{DCn}.sin(k\pi D_n), \tag{2.b}$$

where D_n is the equivalent duty cycle from 0 to 0.5. $\bar{V}_n$ is a complex number, and $\angle \bar{V}_n$ is its phase considering the origin of the phases (zero phase shift) at the origin of the switching period T_s. Thus, (2.a) gives the relationship between the equivalent duty cycle and the amplitude of the 1st harmonic. The phase can be easily obtained by considering the time delay via:

$$\varphi_n = -\frac{t_{Dn}}{T_S}\cdot 360° = -\frac{\omega_0\, t_{D\,n}}{2\pi}\cdot 360°, \tag{3}$$

where t_{Dn} is the time delay of the n-th bridge and φ_n is in degrees. The last bridge can be arbitrarily selected as the reference with zero phase shift. Figure 4(b) shows the logic block diagram inside the controller that converts the desired amplitude and phase into duty cycle and time delay. By modulating the duty cycle, the AC/DC bridge produces the desired AC output. Notice that the inputs of the block are $v_d(t)$ and $v_q(t)$, which are the real and imaginary (or in-phase and quadrature) components of the fundamental signal and not the amplitude and phase because this simplifies the control technique.

In Figure 2 the AC circuit is shown. The transformer is connected to all of the AC ports of the DC/AC bridges, which are considered as voltage sources as Figure 3(a) shows. The following analysis is performed based on the fundamental harmonic, but it can be easily extended to any other harmonic.

According to Figure 3(b), the impedance matrix is obtained. Using the impedance matrix, $\bar{\bar{Z}}$, the voltage at each AC port can be calculated based on the current in each AC port:

$$\vec{V}.e^{j\omega_0 t} = \bar{\bar{Z}} \cdot \vec{I}.e^{j\omega_0 t} \tag{4}$$

where

$$\bar{\bar{Z}} = \begin{pmatrix} j\omega_0(L_{s1}+L_m)+r_{s1} & j\omega_0 L_m & \dots & j\omega_0 L_m \\ j\omega_0 L_m & j\omega_0(L_{s2}+L_m)+r_{s2} & j\omega_0 L_m & \vdots \\ \vdots & j\omega_0 L_m & \ddots & j\omega_0 L_m \\ j\omega_0 L_m & \dots & j\omega_0 L_m & j\omega_0(L_{sN}+L_m)+r_{sN} \end{pmatrix} \in \mathbb{C}^{NxN}$$

$$\vec{V} = \begin{pmatrix} \overline{V}_1 & \overline{V}_2 \dots \overline{V}_N \end{pmatrix}^T \in \mathbb{C}^{Nx1}$$

$$\vec{I} = \begin{pmatrix} \overline{I}_1 & \overline{I}_2 \dots \overline{I}_N \end{pmatrix}^T \in \mathbb{C}^{Nx1}$$

where ω_0 is the fundamental frequency, in our case is also the switching frequency of the converter, $\omega_0 = \omega_s$. The AC voltages and currents are grouped into the complex vectors $\vec{V}$ and $\vec{I}$. A single line above a symbol denotes a scalar complex variable, while an arrow denotes a vector and a double line a matrix. The impedance matrix can be decomposed as:

$$\bar{\bar{Z}} = j\omega_0.\bar{\bar{L}} + \bar{\bar{r}} \tag{5}$$

where $\bar{\bar{L}}$ is inductance matrix (a symmetric matrix) and $\bar{\bar{r}}$ is the resistive matrix (a diagonal matrix). In addition, if we neglect the losses ($\bar{\bar{r}} = 0$):

$$\vec{I} \approx \bar{\bar{Z}}^{-1}.\vec{V} = \bar{\bar{Y}}.\vec{V} = \frac{\bar{\bar{L}}^{-1}}{j\omega_0}.\vec{V}. \tag{6}$$

The admittance matrix is $\bar{\bar{Y}} = \frac{\bar{\bar{L}}^{-1}}{j\omega_o}$ for steady-state sinusoidal waveforms. The vector of complex powers is:

$$\vec{S} = \frac{\vec{V}.\overrightarrow{I^*}}{2} = \frac{j.\vec{V}.\bar{\bar{L}}^{-1}.\overrightarrow{V^*}}{2\omega_0} = [S_1 \quad \dots \quad S_N]^T. \tag{7}$$

where each component is the complex power of each port. Thus, by controlling the amplitude and phase (or real and imaginary parts) of the voltage at each AC port, it is possible to control the power flow. One of the aims of the converter is to transfer power between different ports efficiently, this includes reducing the reactive power, and this is why it is important to measure both active and reactive power.

To conclude, the power through the converter can be controllable based on the AC port voltages according to (7), and these voltages are controllable based on (2) and (3).

Dynamic linear analysis. This analysis considers that the signals vary in order to obtain a dynamic model. The analysis is used to propose a decoupling block and a control loop. The system plant consists of a transformer in its linear range and DC/AC

bridges in which the DC voltages vary smoothly, so they are assumed constant. Thus, the plant is linear and the analysis can be extended to large signals. In order to include the dynamics, (4) needs to be re-written:

$$\bar{\bar{L}}.\frac{d\left(\vec{I}.e^{j\omega_0 t}\right)}{dt}+\bar{\bar{r}}.\vec{I}.e^{j\omega_0 t}=\vec{V}.e^{j\omega_0 t}, \tag{8.a}$$

which is the equation of each port of the transformer in the stationary reference frame. In Laplace domain, considering that the signals vary, they are expressed as $\vec{v}=\vec{V}(s)$ and $\vec{\imath}=\vec{I}(s)$, where s is the Laplace variable. Using rotational reference frame (dq-frame), complex exponentials appear in all of the terms and can be removed:

$$\left(s\bar{\bar{L}}+\bar{\bar{r}}+j\omega_0.\bar{\bar{L}}\right).\vec{\imath}=\vec{v}. \tag{8.b}$$

Notice that the equation has real and imaginary parts. Small letters express variables in Laplace domain. The magnetizing inductance of the transformer (L_m) is omitted because L_m>>L_{sn} and it can be considered as a second order effect. Thus, the sum of the ampere-turns, including all of the windings in the ideal inner transformer, is zero:

$$\sum_{n=1}^{N} n_n\cdot\bar{\imath}_n\approx 0. \tag{9}$$

Therefore, using (9) and considering the N-th port as the fixed reference, the matrices $\bar{\bar{L}}$ and $\bar{\bar{r}}$ can be reduced. The expansion of (8.b), which includes (9), shows that:

$$\left(s\bar{\bar{L}}+\bar{\bar{r}}+j\omega_0.\bar{\bar{L}}\right).\begin{pmatrix}\bar{\imath}_1\\ \bar{\imath}_2\\ \vdots\\ \dfrac{-\sum_{n=1}^{N-1}n_n\cdot\bar{\imath}_n}{n_N}\end{pmatrix}=\begin{pmatrix}\bar{v}_1\\ \bar{v}_2\\ \vdots\\ \bar{v}_N\end{pmatrix}, \tag{10}$$

where lowercase letters with upper lines mean small perturbations in complex variables (voltages and currents). In addition, if $\bar{v}_N$=V_N is the fixed real reference, the last row can be subtracted from the other rows:

$$\left[(s+j\omega_0).\underbrace{\begin{pmatrix}L_{11}^R & \cdots & L_{1(N-1)}^R\\ \vdots & \ddots & \vdots\\ L_{(N-1)1}^R & \cdots & L_{(N-1)(N-1)}^R\end{pmatrix}}_{\bar{\bar{L}}^R}+\bar{\bar{r}}^R\right].\underbrace{\begin{pmatrix}\bar{\imath}_1\\ \vdots\\ \bar{\imath}_{N-1}\end{pmatrix}}_{\overrightarrow{\imath^R}}=\underbrace{\begin{pmatrix}\overline{v_1}-\overline{V_N}\\ \vdots\\ \bar{v}_{N-1}-\overline{V_N}\end{pmatrix}}_{\overrightarrow{v^R}}, \tag{11.a}$$

$$\left[(s+j\omega_0).\bar{\bar{L}}^R+\bar{\bar{r}}^R\right].\overrightarrow{\imath^R}=\overrightarrow{v^R}\in\mathbb{C}^{(N-1)x1} \tag{11.b}$$

where the upper index 'R' means reduced matrices $\in\mathbb{C}^{(N-1)x(N-1)}$ or vectors $\in\mathbb{C}^{(N-1)x1}$. As an example, in a three-port converter with a unitary transformer turns-ratio (n_1=n_2=n_3), leakage inductances L_{s1}, L_{s2} and L_{s3}, and magnetizing inductance L_m, the matrix $\bar{\bar{L}}$ is:

$$\bar{\bar{L}}=\begin{pmatrix}L_{s1}+L_m & L_m & L_m\\ L_m & L_{s2}+L_m & L_m\\ L_m & L_m & L_{s3}+L_m\end{pmatrix} \tag{12}$$

and the reduced matrices are:

$$\bar{\bar{L}}^R = \begin{pmatrix} L_{s1}+L_{s3} & L_{s3} \\ L_{s3} & L_{s2}+L_{s3} \end{pmatrix} \text{ and } \bar{\bar{r}}^R = \begin{pmatrix} r_{s1}+r_{s3} & r_{s3} \\ r_{s3} & r_{s2}+r_{s3} \end{pmatrix}. \quad (13)$$

By using the reduced equations, the current $\overrightarrow{\imath^R}$ can be controlled, which means that currents can be controlled in all ports but one. However, due to $\bar{\bar{L}}^R$ and $\bar{\bar{r}}^R$, the voltage at each port influences the others. Therefore, a decoupling block is needed to provide independence to each port. By achieving that, the control loops will only be a combination of single-input-single-output control loops in parallel. In addition, as the signals are complex variables there is also a coupling between real and imaginary parts due to the "$j\omega_0$" term. Figure 5(a) shows the block diagram of the power stage, where the inputs are the AC voltages of each bridge and the outputs are the AC currents in each bridge, based on (11.b). Real and imaginary (dq) components of $\vec{v} = \overrightarrow{v_d} + j\overrightarrow{v_q}$ and $\vec{\imath} = \overrightarrow{\imath_d} + j\overrightarrow{\imath_q}$ are used. For that (11.b) is decomposed in its dq-frame representation, and this is the plant model:

$$\begin{aligned} \overrightarrow{\imath_d^R} &= \left(s.\bar{\bar{L}}^R + \bar{\bar{r}}^R\right)^{-1}\overrightarrow{v_d^R} + \omega_0.\bar{\bar{L}}^R.\overrightarrow{\imath_q^R} \\ \overrightarrow{\imath_q^R} &= \left(s.\bar{\bar{L}}^R + \bar{\bar{r}}^R\right)^{-1}\overrightarrow{v_q^R} - \omega_0.\bar{\bar{L}}^R.\overrightarrow{\imath_d^R}. \end{aligned} \quad (14)$$

Development of control algorithms for MAB converters using dq-frame representation. In order to control $\overrightarrow{\imath_d}$ and $\overrightarrow{\imath_q}$ independently in each AC port, the controller must have a decoupling block. The idea is to create an auxiliary complex vector, $\vec{u} = \overrightarrow{u_d} + j\overrightarrow{u_q}$ in which each component affects only to an exact AC (real or imaginary) current at a certain port. For that, based on (14), the non-coupled current terms are grouped in one side of the equations while the other side can be replaced by the auxiliary control vector:

$$\left(s\bar{\bar{r}}^{R^{-1}}.\bar{\bar{L}}^R + \bar{\bar{I}}\right)\overrightarrow{\imath^R}(s) = \left[-j\omega_0\bar{\bar{r}}^{R^{-1}}.\bar{\bar{L}}^R.\overrightarrow{\imath^R}(s) + \bar{\bar{r}}^{R^{-1}}.\overrightarrow{v^R}(s)\right] = \vec{u}, \quad (15.a)$$

where $\bar{\bar{I}}$ is the identity matrix. Thus, $\vec{u}$ is defined and has ampere units, and so, $\overrightarrow{v^R}$ can be defined in terms of $\vec{u}$ as:

$$\overrightarrow{v^R} = \left[j\omega_0.\bar{\bar{L}}^R\overrightarrow{\imath^R}(s) + \bar{\bar{r}}^R\vec{u}\right]. \quad (15.b)$$

Finally, using $\vec{u}$, the transfer function $\overrightarrow{\imath^R}/\vec{u}$ (s), from (15.a) is:

$$\overrightarrow{\imath^R}(s) = \left(s\underbrace{\bar{\bar{r}}^{R^{-1}}\bar{\bar{L}}^R}_{\bar{\bar{T}}} + \bar{\bar{I}}\right)^{-1}\vec{u} \quad (16)$$

If the matrix in (16) is diagonal, then each u-component controls independently each i^R-component in both real and imaginary parts. Therefore, it is important to have a diagonal matrix in (16). For that, $\bar{\bar{T}} = \bar{\bar{r}}^{R^{-1}}.\bar{\bar{L}}^R$ should be diagonal. To obtain a diagonal matrix, the ratio between leakage inductance, L_{sn}, and series resistance, r_{sn}, of each winding—or, in other words, the time constants of the windings—must be the same. Two possible controls can be applied: 1) when the windings' time constants are equal or 2) when they are unequal.

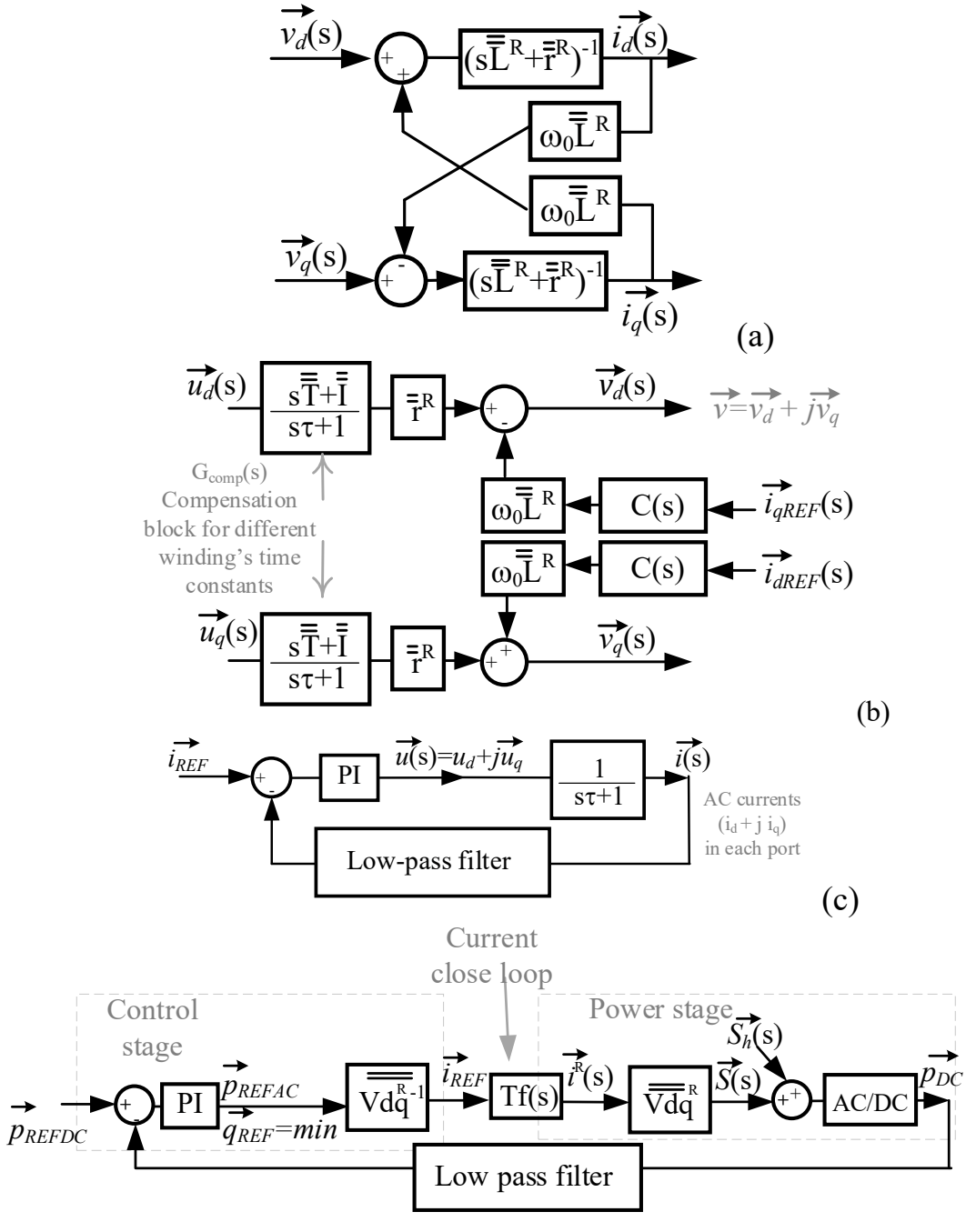

Figure 5- Control diagram: (a) (coupling) power stage, (b) decoupling control stage, (c) equivalent current loop diagram and (d) DC power control loop

Equal time constants*:* $\bar{\bar{T}} = \tau\bar{\bar{I}}$*:* according to (16), defining $\tau = L_{sn}/r_{sn}$, and to keep the plant as a single-pole transfer function, the current is controlled by $\vec{u}$ as:

$$\overrightarrow{\imath^R}(s) = \left(s\bar{\bar{T}} + \bar{\bar{I}}\right)^{-1}\vec{u} = \left(s\tau\bar{\bar{I}} + \bar{\bar{I}}\right)^{-1}\vec{u} = \frac{\vec{u}}{s\tau + 1}. \quad (17)$$

Therefore, from the point of view of $\vec{u}$, this implies an independent first order plant per component. For achieving that, the decoupling equation (15.b) is used. A block diagram that clarifies the decoupling block is presented in Figure 5(b). Notice

that by combining both the decoupling block and the power stage from (14) also depicted in Figure 5(a), the coupling effects are cancelled and the i^R-components follow the u-components through the first order system. For the diagram, the dq-components were extracted from (15.b), in a similar manner that (14) from (11.b). As the decoupling is not always equal than the coupling the perfect match is not achieved. Details are included in [A17].

Non-equal time constants*:* If the time constants are not the same, (16) has coupling effects between the ports based on the matrix transfer function $\frac{\overrightarrow{\imath^R}}{\vec{u}(s)} = \left(s\bar{\bar{T}} + \bar{\bar{I}}\right)^{-1}$. The solution for that is to add a compensation block before $\vec{u}(s)$:

$$G_{comp}(s) \approx \frac{\left(s\bar{\bar{T}} + \bar{\bar{I}}\right)}{s\tau + 1}. \tag{18.a}$$

Then $\vec{u}$ is replaced by $\vec{u}'$

$$\vec{u}'^{(s)} = G_{comp}(s)\vec{u}(s). \tag{18.b}$$

Thus, (16) becomes:

$$\overrightarrow{\imath^R}(s) = \left(s\bar{\bar{T}} + \bar{\bar{I}}\right)^{-1}\vec{u}' \approx \left(s\bar{\bar{T}} + \bar{\bar{I}}\right)^{-1}\frac{\left(s\bar{\bar{T}} + \bar{\bar{I}}\right)}{s\tau + 1}\vec{u} \approx \frac{\vec{u}}{s\tau + 1}. \tag{19}$$

The equation is approximated because the matching between poles and zeros is not perfect due to measurement errors. Figure 5(b) shows the compensation blocks in the control chain. Note that (19) shows that the $\overrightarrow{\imath^R}(s)$ and $\vec{u}$ are linked with a simple transfer function which is single-input-single-output (SISO). There is a SISO transfer function for each current at each port. Thus, to control them, a simple controller can be implemented plus some algebraic equations which allows decoupling of the d and q components at each port. These equations (controller and decoupling block) are simple and can be easily implemented discretely in a microprocessor. Therefore, this new technique allows extending the converter to work with any number of ports because the processing time of a digital proportional-integral (PI) controller with the decoupling block is only several microseconds in a microprocessor.

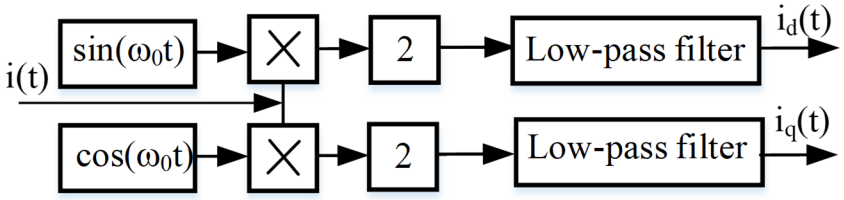

Figure 6- dq-transformation for AC currents

Current control loop. Having modeled the power stage (coupling block) and proposing the decoupling block, the next step is to close the loop and control $\overrightarrow{\imath^R}$. For that, by joining Figure 5(a) and Figure 5(b), a simple control block diagram is obtained in Figure 5(c). There, the plant is the combination of the power stage and the decoupling stage and it is governed by $\vec{u}$. In addition, in the feedback loop, the currents are measured using the transformation block from Figure 6. Notice that this block is

working with analog multipliers and analog filters [A2][A17]. The low-pass filter (LPF) can be first or second order because it needs to filter frequencies higher than twice the switching frequency while keeping the DC components (i_d and i_q) unchanged.

The design of the control loop involves the selection of the controller. In this case, a simple PI controller is suggested. The open loop transfer function for current control, OL_{Tf_C}, is:

$$OL_{Tf_C}(s) = k_{P_c}\frac{sT_{i_c}+1}{sT_{i_c}}\frac{1}{s\tau+1}LPF(s), \tag{20}$$

where T_{iC} is the integration time constant and k_{Pc} is the proportional constant of the PI controller. The low-pass filter can be written as:

$$LPF(s) = \frac{1}{\left(\frac{s}{\omega_{c_c}}\right)+1}, \tag{21}$$

where ω_{c_c} is the cut-off frequency of the filter. The plant is represented according to (17-19). A simple approach indicates that if T_{iC} cancels the plant time constant, $\tau=L_{sn}/r_n$, the order of the system is reduced. Then, to select k_{Pc} a conservative approach is to set the frequency corresponding to the 0dB open-loop, ω_{0dB}, far from the filter cut-off frequency, ω_{c_c}, so by using (20) and neglecting the low pass filter:

$$\omega_{0dB} \approx \frac{k_{P_c}}{T_{i_c}}. \tag{22}$$

Thus, the approximate closed-loop transfer function for the current control, CL_{Tf_C}, in the control region will be (for a 1st order measurement filter):

$$CL_{Tf_C}(s) = \frac{1}{s\frac{T_{i_c}}{k_{P_c}}+\frac{1}{1+\frac{s}{\omega_{c_c}}}} \tag{23}$$

and, if the plant pole is dominant, $\omega_{0dB} << \omega_{c_c}$, it can be approximated to:

$$CL_{Tf_C}(s) = Tf(s) \approx \frac{1}{1+s\underbrace{\left(\frac{T_{i_c}}{k_{P_c}}\right)}_{\omega_{0dB}}}. \tag{24}$$

Because, within the bandwidth the filter $LPF(s) \approx 1$. Based on this control loop in each AC port and for real and imaginary parts, an AC power control loop can be implemented straight forward. By using the dominant pole approximation (24), the closed-loop transfer function $\frac{i^R}{I^R_{REF}}(s)$ for any d and q components and at any port can be considered as a first order system. This will be used in the secondary control loop.

AC power calculation. Being able to control the currents, since the voltages are well-known, active and reactive powers can also be controlled. The AC power at the n-th port is:

$$\bar{S}_n = \overline{v_n}.\overline{i_n}^*/2 = \left(v_{nd}+jv_{nq}\right).\left(i_{nd}-ji_{nq}\right)/2 \tag{25}$$

$$\begin{pmatrix} P_n \\ Q_n \end{pmatrix} = \underbrace{\begin{pmatrix} v_{nd}/2 & v_{nq}/2 \\ v_{nq}/2 & -v_{nd}/2 \end{pmatrix}}_{\overline{\overline{V_{dq_1}}}} \cdot \begin{pmatrix} i_{nd} \\ i_{nq} \end{pmatrix}. \tag{26}$$

Therefore, the AC power calculation block must extract the current references as:

$$\begin{pmatrix} i_{nd_{ref}} \\ i_{nq_{ref}} \end{pmatrix} = \frac{2\begin{pmatrix} v_{nd} & v_{nq} \\ v_{nq} & -v_{nd} \end{pmatrix}}{\left({v_{nd}}^2 + {v_{nq}}^2\right)} \cdot \begin{pmatrix} P_{n_{ref}} \\ Q_{n_{ref}} \end{pmatrix} \tag{27}$$

where v_{nd} and v_{nq} represent the voltage in the d- and q-axis of the n^{th} bridge respectively. This block is included in the final control loop as "V_{dq}^{-1}", see Figure 5 (d). Note that, both active and reactive power can be controlled. Active power is useful for transferring power at the DC ports. Reactive power can be used for achieving zero-voltage switching (ZVS). The reactive power lags the current phase so the switches can turn-on while the current is still negative and the ZVS is achieved using the anti-parallel diodes. The amount of reactive power depends on the needed phase shift.

DC Power controller – the secondary controller. A DC power controller is implemented for improving the accuracy of the DC power transfer due to the effect of the power in the harmonic signals which are not under control and can be considered as an external perturbation. The DC power is controlled at each DC port using measurement units (sensors) and DC power references that provide the proper AC references for the inner loop. Figure 5(d) shows the block diagram of the outer control loop. The design of the control loop is similar to the current control loop. Voltage blocks do not add any dynamics, the transfer function Tf(s) from the current loop and some extra delays due to the DC power measurements must be considered.

Computer simulations: quadruple active bridge (QAB). As an example, to test the proposed method, let us consider a 4-port active bridge (QAB), it might be the case illustrated in Figure 1 in which all of the ports have bidirectional power flow. It is convenient that all the QAB magnetic components have the same time constant $\tau=L_n/r_n$ as was explained in Section 2.3. Thus, the poles of each winding are located in the same place which simplifies the controller. This can be achieved with a special design of the magnetic components, designing a single transformer or a set of inductors and a transformer [A23].

In order to design the control loops: (inner) dq-frame current-control loop and DC power-control loop, the diagrams in Figure 5(c) and 5(d) were used. Eq. (20) is used considering that the decoupling network in Figure 5(b) matches the coupling network in Figure 5(a). For this example, the values are shown in Table 1 and ω_{0dB} was set at $0.1\omega_{Cc}$, thus (24) is valid and the design procedure follows Section 2.3.

The open-loop current-control transfer function frequency response of one port is shown in Figure. 7(a): $i_{d1}^R/(I_{dREF1}^R - i_{d1}^R)$. All other ports have the same transfer function because they have the same time constants. The simulations include a time delay ($1.5/f_S$) due to the discretization and PWM techniques and this is why the phase is continuously growing. Two curves are shown: a) the dashed curve represents the ideal model where the decoupling block perfectly matches the power plant, and b) the

continuous adds the low pass filter.

Table 1: QAB converter parameters for simulations

Symbol	Quantity	Value
f_s	Switching frequency	40kHz
$V_{DC1,2,3}$	DC Input voltages	650-800 V
$L_{s1,2,3}$	Leakage inductances	20uH
n_1,n_2,n_3	Windings' turns-ratio	1
$r_{s1,2,3}$	Windings' resistances	0.3Ω
$\omega_{C\,c}$	Cut-off freq. for low-pass filter in dq-transformation	$2\pi f_s/5$
ω_{0dB}	Frequency at 0dB open current loop gain	5 krad/s
L_m	Magnetizing inductance	1mH
$T_{i\,c}$	Current controller integration time	0.07ms
$k_{P\,c}$	Current controller proportional gain	0.33
$T_{i\,p}$	Power controller integration time	0.2ms
$k_{P\,p}$	Power controller proportional gain	0.5
$\omega_{C\,p}$	Cut-off freq. for low-pass filter in power calculation	$2\pi f_s/5$

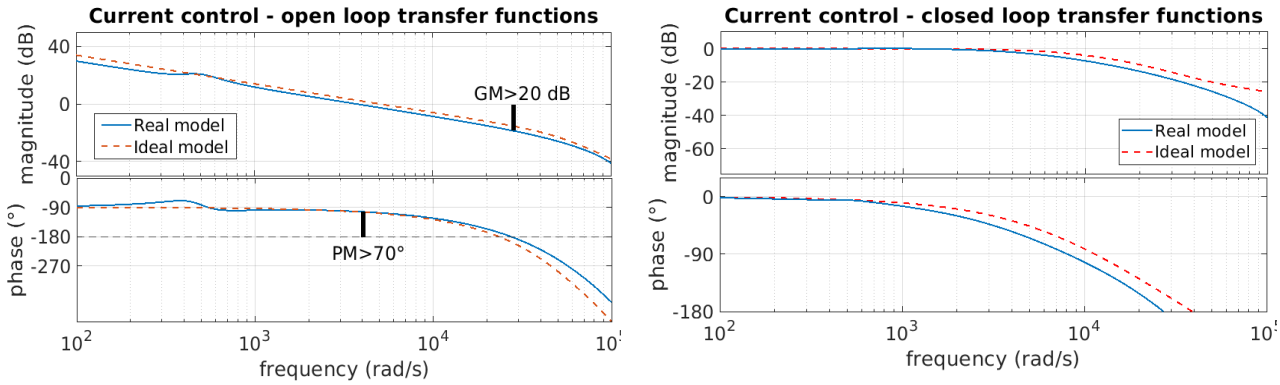

(a) (b)

Figure. 7- Frequency response plot of (a) the open-loop current loop, $i_{d1}{}^R/(I_{dREF1}{}^R-i_{d1}{}^R)$ and (b) closed-loop transfer function, $i_{d1}{}^R/I_{dREF1}{}^R$. The ideal model is the model which was considered in the design guide with exact decoupling

Once the current loop is designed, the next step is the DC power controller design. For that the closed-loop current control transfer function "Tf(s)" is needed (shown in Figure. 7(b)). A simplified model follows (24) and the same transfer function can be obtained for all other currents of the QAB ($I_{d3}^R, I_{q3}^R I_{d2}^R, I_{q2}^R, I_{q1}^R$).

For obtaining the AC power, the V_{dq} block was added in Figure 5(d) to get the power corresponding to the 1st harmonic approximation. However, as some vestigial power is on the harmonics, the control loop is on the DC power as shown in Figure 5(d). Due to the measurements and the DC capacitors a delay exists for measuring DC power, thus another filter is considered, $LPF_P(s)$. The open-loop transfer function of the complete DC power control scheme is:

$$OL\,Tf_P(s) = k_{P_P}\frac{sT_{i_P+1}}{sT_{i_P}}\frac{1}{\frac{s}{\omega_{0dB}}+1}LPF_P(s), \tag{28}$$

where the sub-index P means DC power control loop. In this case, the filter transfer function can be considered out of the bandwidth, the pole at ω_{0dB} can be cancelled with the PI pole (ω_{0dB} =1/$T_{i\,p}$), and finally the $k_{P\,p}$ is adjusted to the desired bandwidth. In order to validate this control system, several simulations based on the proposed model.

In order to test the converter a power step was performed. The initial power per port was: P_{DC1}=10kW, P_{DC2}=5kW, P_{DC3}=0kW and P_{DC4} balances the power. After 5ms, the power changes to P_{DC1}=2.5kW, P_{DC2}= P_{DC3}=-5kW. Figure 8(a) shows the results; the time response is about 2ms and the power control is accurate. In addition, Figure 8(b) shows a similar case but when the transformer windings' time constants are different because of different leakage inductances: L_{s1}=10uH, L_{s2}=20uH, L_{s3}=30uH and L_{s4}=20uH. The results show that the time response is about 5ms, slightly slower than the case of equal inductances but the system is still working properly.

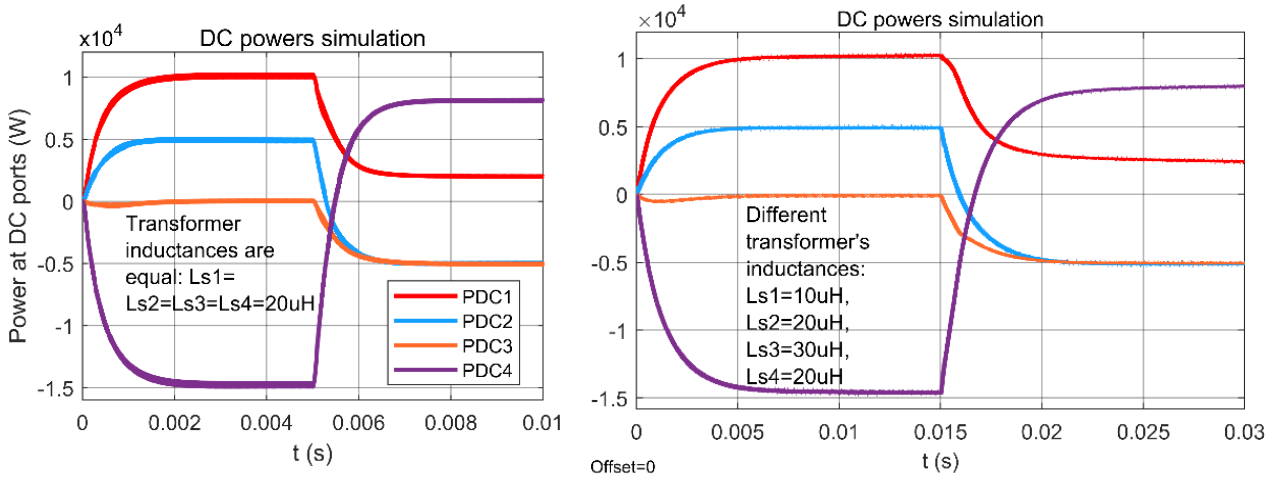

Figure 8- Simulations using DC power control diagram (a) power response after a step in the references and (b) dq-frame currents

Figure 9 shows the simulation waveforms for the proposed approach at two different power operational points, at the end of each interval shown in Figure 8: interval 1) P_{DC1}=10kW, P_{DC2}=5kW, P_{DC3}=0kW and interval 2) P_{DC1}=2.5kW, P_{DC2}= P_{DC3}=-5kW. Notice that port one, three and four are at V_{DC1}=V_{DC3}=V_{DC4}=650V while V_{DC2}=800V, in order to show that the converter can work at different voltages as well with different duty cycles. Figure 9(a) shows the voltages in each AC port, Figure 9(b) shows the AC current waveforms and Figure 9(c) shows the DC currents in each DC port.

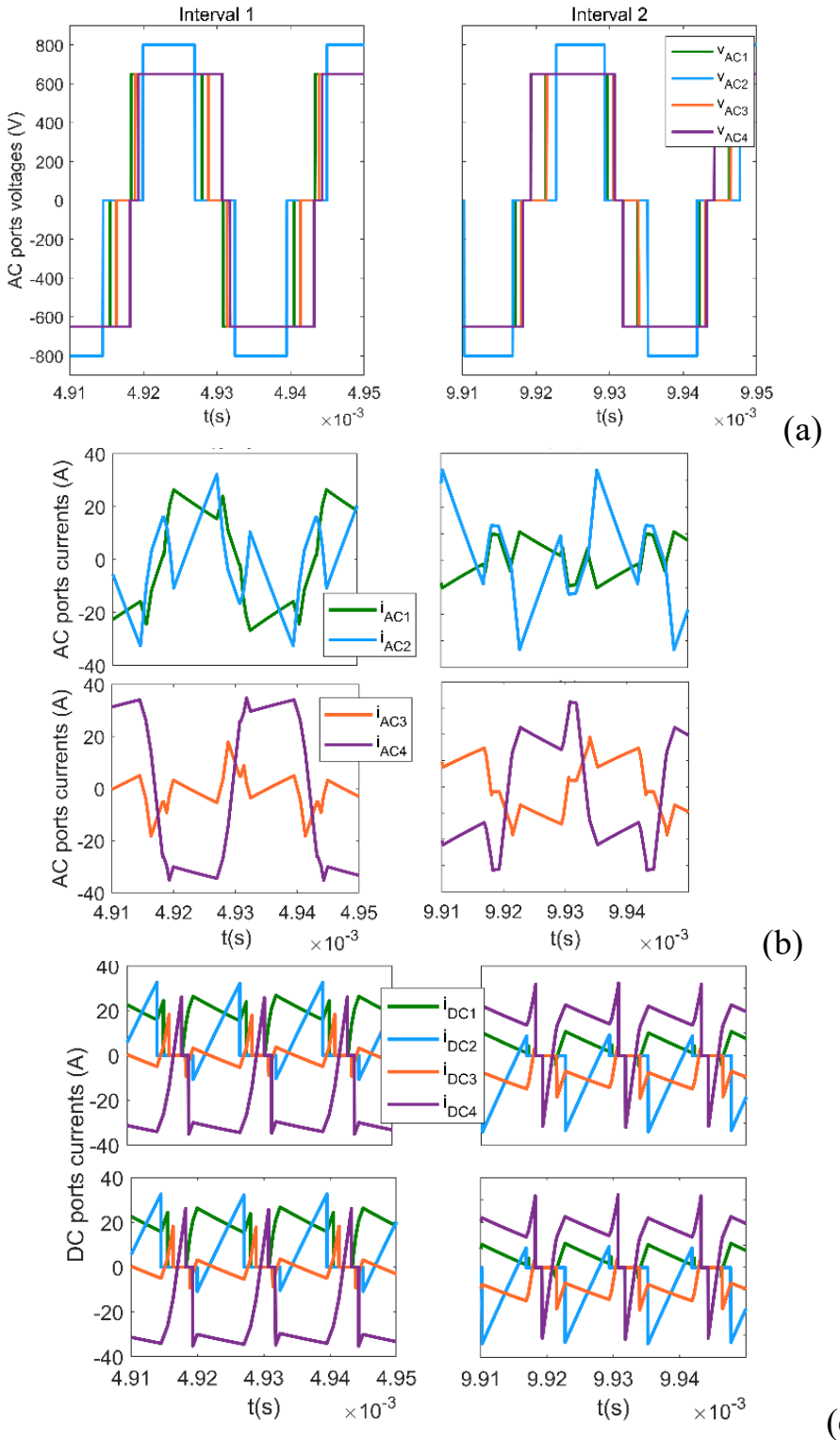

Figure 9- Simulation waveforms at different power and voltages: (a) AC voltages, (b) AC currents and (c) DC currents

Experimental results. In order to validate the proposed control, a 400W- triple active bridge (TAB) converter was built and tested, see Figure 10. The main circuit consists of three bridges connected to a transformer and controlled with a driver stage. A controller (microprocessor) sends the gate signals to the drivers and receives all the

information using current sensors. Table 2 lists the details of the converter. The dq-decomposition is done using an analogue multiplier and a set of filters as shown in Figure 6. Finally, all of the measurements go to the analogue-to-digital units into the microprocessor.

Table 2: Triple Active Bridge, Prototype parameters

Symbol	Quantity	Value
f_s	Switching frequency	40kHz
$V_{DC1,2,3}$	DC Input voltages	150-220 V
$L_{s1,2,3}$	Leakage and external inductances	28uH, 26uH, 28uH
n_1,n_2,n_3	Windings' turns-ratio	1
$r_{s1,2,3}$	Windings' resistances	0.2Ω
ω_{C_c}	Cut-off freq. for low-pass filter in dq-transformation (Fig. 5.d)	$2\pi f_s/5$
	Switches, MOSFETs	IPW60R060
L_m	Magnetizing inductance	1mH

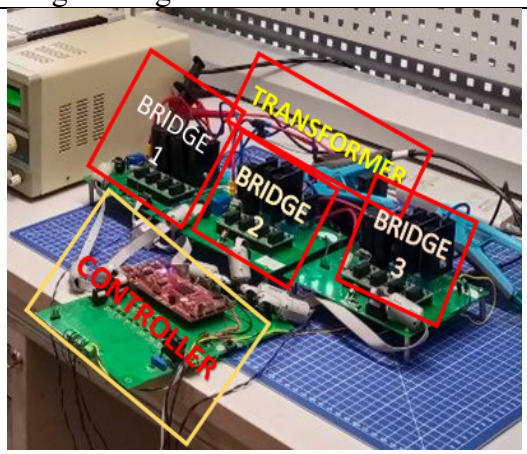

Fig. 10- Prototype

Figure 11(a) shows a power step test which shows the bidirectional behavior of the converter and the time response. In the 1st interval port 1 absorbs 400W and port 2 zero, P_{DC1}=-400W, P_{DC2}=0W. In the 2nd interval both ports deliver the same power P_{DC1}=P_{DC2}=200W, in the 3rd interval P_{DC1} is set to zero while P_{DC2}=400W and finally in the last interval P_{DC2} is set to zero while P_{DC1}=400W. These test covers all of the power flows conditions including positive, zero and negative power flows. The time response is about 8ms for the power loop and the inductances are not equal. Figure 11(b) shows the real waveforms of AC voltage, AC currents and DC currents in three time intervals. The V_{DC} at port 2 is 180V while V_{DC1}=V_{DC3} are 150V. This shows that the converter can work within a voltage range. In addition to the waveforms, an AC power analysis was done to evaluate the active and reactive power are in each harmonic. Results show that mostly all of the power flows at the 1st harmonic and the reactive power is minimal.

This chapter introduces the new model and its validation in simulations and real experiments.

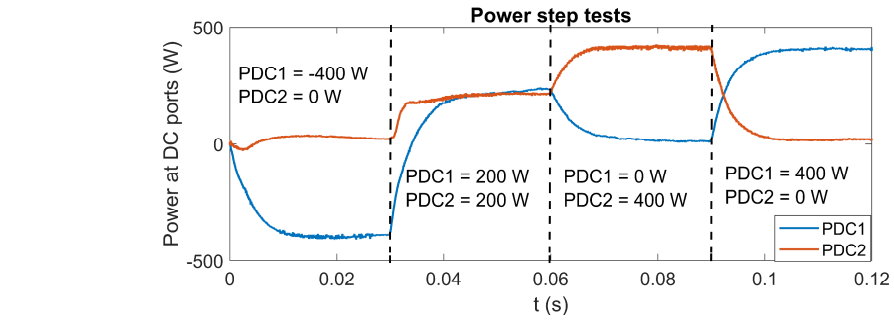

(a)

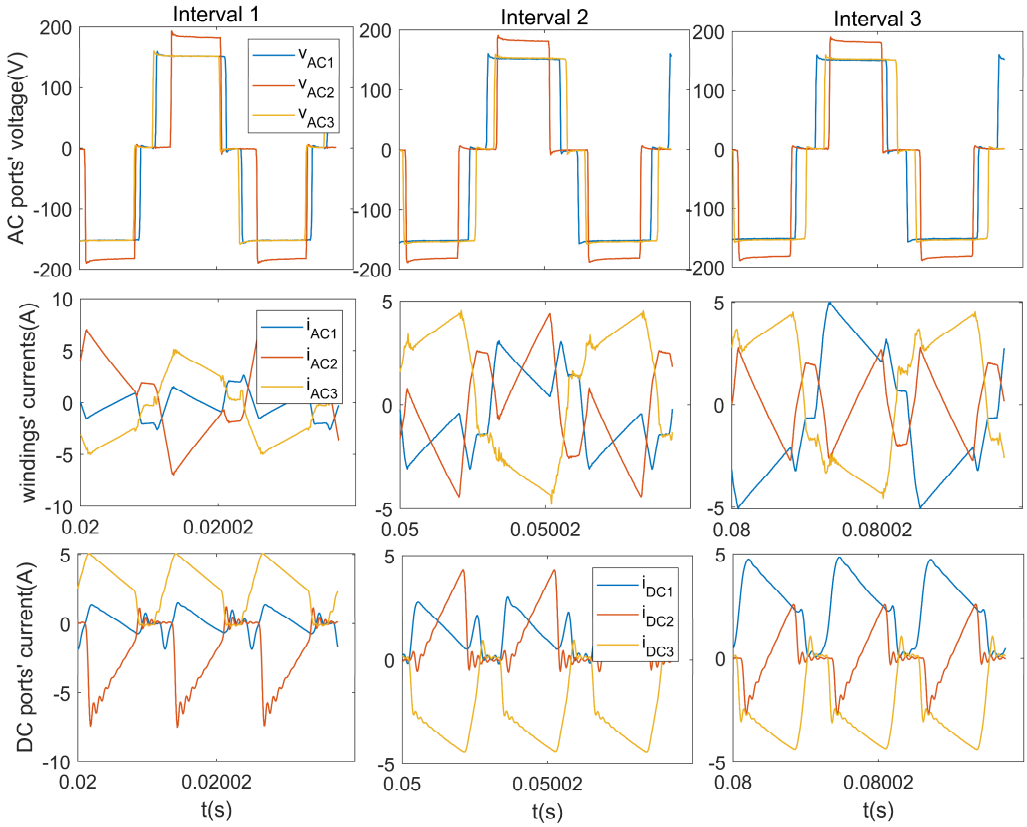

(b)

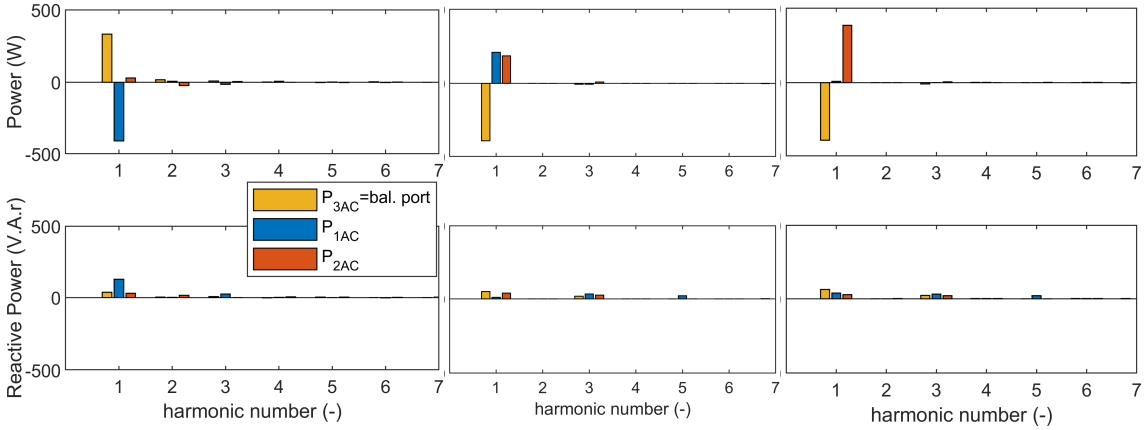

(c)

Figure 11- Power step test: (a) Power at two DC powers when the reference changes to several points: P_{DC1},P_{DC2}=[-400W,0W], [200W,200W], [0W,400W], (b) waveforms within the intervals, (c) AC harmonic active and reactive power distribution

Improvements in efficiency using "dual-duty" modulation. The RMS currents can be reduced using a special modulation technique [A3]. Since the active power is controlled and AC bridges are connected with mostly inductive lines (see chapter 3), the AC ports' voltages have nearly equal first harmonic magnitudes (considering a turns-ratio equals to one). However, the DC port voltages can vary significantly for sources such as battery and supercapacitors. This results in different input voltages V_{DCn} among the different bridges. In this case, to get equal magnitudes $|\overline{V}_n|$ in the AC ports, different duty cycles must be applied.

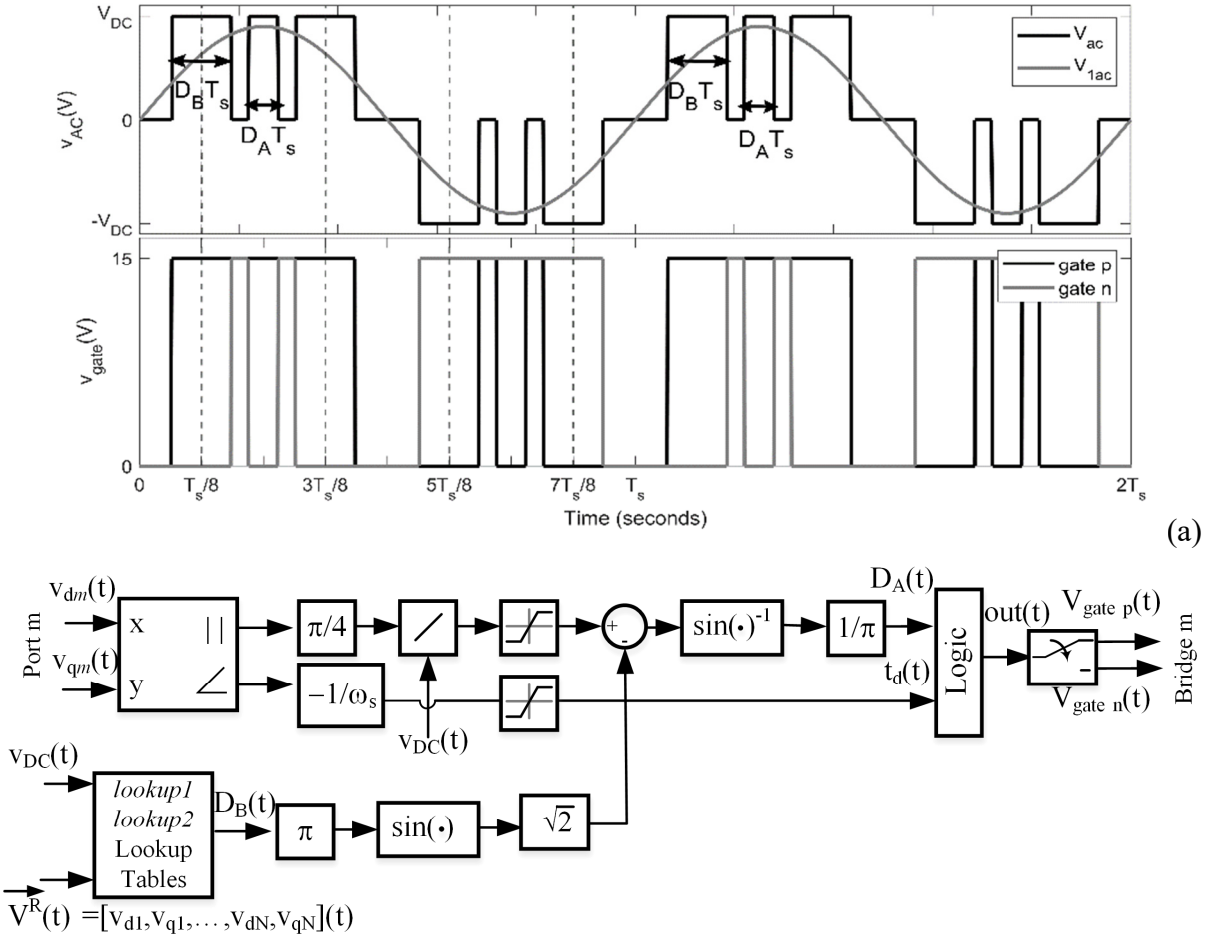

Figure 12- Single bridge diagram: (a) proposed dual-duty modulation, (b) control logic diagram for dual-duty modulation including lookup tables

According to (2.b), different duty cycles lead to different harmonic voltage magnitudes. The difference in magnitudes in turn produces high reactive power from harmonics, which is hard to control. To eliminate this effect, a new modulation technique is introduced, called "dual-duty" modulation, shown in Figure 12(a), with two duty cycles, D_A and D_B [A3]. With $D_B = 0$, PWM signal becomes the same as for the previous (chapter 3) modulation. Thus, D_A is the main duty cycle, and D_B is the secondary one. The secondary duty cycle is then used as an additional degree of freedom. The main objective is to have almost the same harmonic amplitude to minimize the currents at high order harmonics, by means of selecting the appropriate

values of D_A and D_B. Therefore, for the inductive impedance matrix, the reactive power from harmonics will decrease.

The AC output voltages are generated from a combination of two symmetric duty cycle signals in $v_{Gate\ p}$ and $v_{Gate\ n}$ (voltage in the gates of the switches) and their complementary signals (see Figure 12(a)). Three levels of AC output voltage are produced: a positive level, where $v_{Gate\ p}$ is on and $v_{Gate\ n}$ is off; a zero level, where both are on or both are off; and a negative level, where $v_{Gate\ p}$ is off and $v_{Gate\ n}$ is on.

Figure 12(a) shows the gate-pulse waveforms for a single bridge. If $D_B \neq 0$, $v_{Gate\ p}$ is on during time periods $\left[\frac{T_S}{8} - \frac{D_B T_S}{2}, \frac{3T_S}{8} + \frac{D_B T_S}{2}\right]$, $\left[\frac{5T_S}{8} + \frac{D_B T_S}{2}, \frac{3T_S}{4} - \frac{D_A T_S}{2}\right]$, $\left[\frac{3T_S}{4} + \frac{D_A T_S}{2}, \frac{7T_S}{8} - \frac{D_B T_S}{2}\right]$. Otherwise, for $D_B = 0$ (same as in Figure. 4), $v_{Gate\ p}$ is on during time period $\left[\frac{T_S}{4} - \frac{D_A T_S}{2}; \frac{T_S}{4} + \frac{D_A T_S}{2}\right]$. The $v_{Gate\ n}$ signal behaves symmetrically relative to the half of the switching period. The same procedure applies to obtain the gate signals of the other bridges.

Figure 12(b) details the transformation block used for obtaining the gate pulses from the signals in the dq-frame. The logic block first selects the secondary duty cycle D_B to minimize the higher harmonics' contribution, as described further in this section. After that, it calculates the main duty cycle (D_A) and phase shift for the first harmonic from the dq-frame voltages (v_d and v_q). Then, the duty cycles, D_A and D_B, and phase shift are translated into $v_{Gate\ p}$ and $v_{Gate\ n}$. The result is shown in Figure 12(a), where the gate signals ($v_{Gate\ p}$, $v_{Gate\ n}$) and the AC output voltage (v_{ac}) are presented, in addition to the 1st harmonic (v_{1ac}). The equations for the fundamental harmonic and any odd k^{th} harmonic can be written as:

$$\left|\overline{V}_n\right| = \left|\overline{V}_{n1}\right| = \frac{4}{\pi} V_{DCi}\left(sin(\pi D_{An}) + \sqrt{2} sin(\pi D_{Bn})\right), \tag{29.a}$$

$$\left|\overline{V}_{nk}\right| = \frac{4}{\pi k} V_{DCn}\left(sin(k\pi D_{An}) + 2cos\left(\frac{\pi k}{4}\right) sin(k\pi D_{Bn})\right), \tag{29.b}$$

where

$$D_{Bn} + D_{An} < 0.25, \text{ if } D_{Bi} > 0. \tag{29.c}$$

From (32.a), various combinations of the main and secondary duty cycles can be used to generate the same first harmonic voltage. The first harmonic voltage is obtained from the control loop, described in Section 2.2. Thus, we use the secondary duty cycle D_B as an additional degree of freedom for each bridge.

As described earlier, the impedance connecting the bridges is mostly inductive. Thus, the minimal first harmonic reactive power will be achieved with nearly the same voltage magnitudes in each port (so the minimal current). Therefore, we can minimize the harmonic voltage magnitude differences to decrease the reactive power from harmonics.

First, we explain how the harmonic reactive power is minimized between two bridges. After that, we provide the algorithm for any number of bridges. For any given

two bridges *n* (reference bridge) and *p* this can be formulated as an optimization problem:

$$\frac{1}{3}\left(|\overline{V}_{n3}| - |\overline{V}_{p3}|\right)^2 + \frac{1}{5}\left(|\overline{V}_{n5}| - |\overline{V}_{p5}|\right)^2 + \frac{1}{7}\left(|\overline{V}_{n7}| - |\overline{V}_{p7}|\right)^2 \rightarrow min, \tag{30.a}$$

under constraints: (30.b)

$$\frac{4}{\pi}V_{DCn}\left(sin(\pi D_{An}) + \sqrt{2}sin(\pi D_{Bn})\right) \equiv |\overline{V}_{n1}|$$
$$\frac{4}{\pi}V_{DCp}\left(sin(\pi D_{Ap}) + \sqrt{2}sin(\pi D_{Bp})\right) \equiv |\overline{V}_{p1}| \tag{30.c}$$

that are derived from (29.a) and (29.b).

In (30.a), harmonics 3, 5, 7 are considered. $D_{B\,n,p}$ are the optimization variables. $D_{A\,n,p}$ are then uniquely determined by (30.b-c). $\overline{V}_{n1}$, $\overline{V}_{p1}$ are the values calculated by the control loop (see chapter 3). Other harmonic voltages used in (30.a) are calculated from (29.b).

Because the inductive reactance increases with frequency, weighting coefficients $\frac{1}{3}$,$\frac{1}{5}$, $\frac{1}{7}$ are used, higher harmonics contribute less to reactive power. In other words, for the k^{th} harmonic, the impedance matrix in (4.a-b) is multiplied by *k*.

Expanding (33.a) according to (32.b), we can rewrite it as:

$$\sum_{k=3,5,7}\frac{1}{k}\left(\frac{V_{DCn}}{V_{DCp}}y_k(D_{An}, D_{Bp}) - y_k(D_{An}, D_{Bp})\right)^2 \rightarrow min, \tag{31.a}$$

where: (31.b)

$$y_k(D_A, D_B) \equiv \frac{1}{k}\left(sin(k\pi D_A) + 2cos\left(\frac{\pi k}{4}\right)sin(k\pi D_B)\right).$$

From the equations (30.b-c), (31) and assuming that $|\overline{V}_{n1}| \approx |\overline{V}_{p1}| \approx |\overline{V}_{AC}|$ we can claim that optimal secondary duty cycles $D_{B\,n,p}$ depend on $\frac{V_{DCn}}{|\overline{V}_{AC}|}$, $\frac{V_{DCn}}{V_{DCp}}$ ratios. Thus, we can precalculate the optimal values and store them in lookup tables. For our proposed control, we define two lookup tables. Table *lookup1* is two-dimensional with the aforementioned parameters (ratios) as inputs. It is used when both D_{Bn} and D_{Bp} are unknown. For the cases when D_{Bn} is known, we create another table *lookup2* with D_{Bn} as 3rd dimension.

The overall algorithm for calculating the main (D_{An}) and secondary (D_{Bn}) duty cycles is the following:

(a) Find bridges with maximum and minimum input voltages, V_{DCmax} and V_{DCmin} respectively. Determine $D_{B\,vmax}$ and $D_{B\,vmin}$ using table *lookup1*.

(b) For any other bridge "*t*", to apply the same technique as with two bridges, first determine the reference bridge (*n*). If $(V_{DCmax} - V_{DC\,t}) > (V_{DC\,t} - V_{DCmin})$, then the reference bridge (*n*) is the one with V_{DCmax}, otherwise, select the bridge with V_{DCmin} as the reference bridge (*n*).

(c) For the bridge "*t*", find D_{Bt} using table *lookup2* with $\frac{V_{DCn}}{|\overline{V}_{AC}|}, \frac{V_{DCn}}{V_{DCt}}$ and D_{Bn} as input parameters.

(d) Using (29.a), calculate main duty cycles D_{At} to get the exact desired fundamental harmonic voltages $|\overline{V}_{t1}|$ for each bridge. These come from the control loop, as described in Section 2.2.

(e) If for bridge *"t"* (29.c) is not satisfied, then bridge "*t*" works in the single-duty mode with duty cycle calculated from (2) and D_{Bt}=0.

The common structure of the dual-duty optimization is shown in Figure 12(b).

One of the benefits of the proposed algorithm is that it is easy to scale. The size and the values of the lookup tables depend only on the normalized AC and DC voltage ranges, and do not depend on the number of ports. First, the harmonic power is optimized between the bridges with minimum and maximum input voltages (n and p). The other bridges are optimized relative to the bridge with the largest V_{DCn-p} difference. It is important to note that this algorithm is heuristic and may not always provide a globally optimal solution. However, it is designed to ensure scalability. To solve the full optimization problem, all DC voltages would need to be indexed in a lookup table.

While it may initially appear that storing a two-dimensional and a three-dimensional table could consume a significant amount of memory, this concern is mitigated by the relatively small ranges of the indexes. For instance, with the $\frac{V_{DCn}}{V_{DCp}}$ ratio limited to 1.5, and step size of 0.05 for all the parameters, the size of tables *lookup1* and *lookup2* would be 14x11x2 (for both $D_{B\ vmax}$ and $D_{B\ vmin}$) and 6x14x17, respectively. These dimensions are suitable for storage in a moderate-sized digital signal processor (DSP), and these sizes will not change with the increased number of bridges.

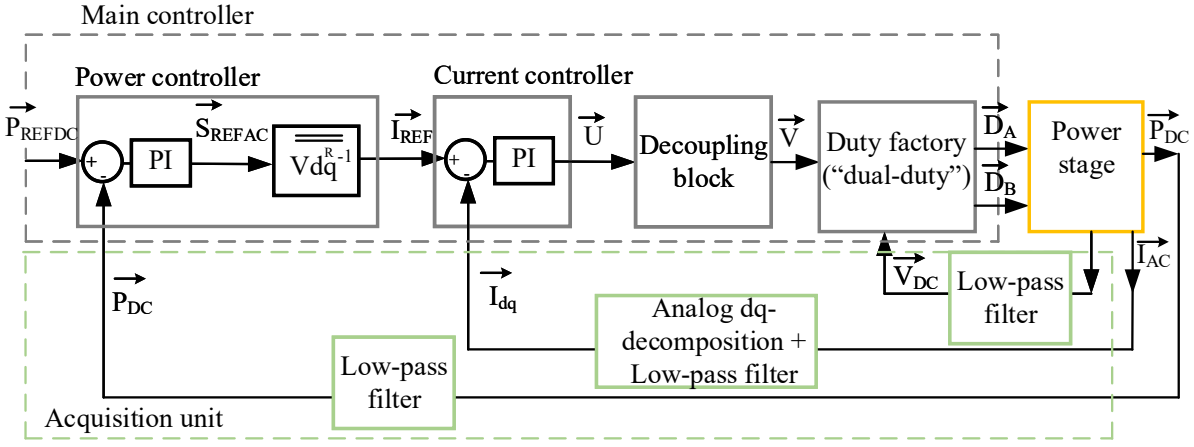

Figure 13- Complete block diagram of the proposed solution

The components of the converter with the proposed control technique are illustrated in Figure 13. The overall proposed method includes the advanced modulation technique ("duty factory" block) that improves the harmonic impact of the currents, the dynamic control technique (power and current controllers) that forms the

dq-frame voltages for the duty factory and the acquisition unit (analog dq-decomposition + low-pass filter, detailed in Figure 6). The power stage was already depicted in Figure. 2. The converter's dynamic that includes the rest of the blocks was presented in Section 2.2. The duty factory block is described in this Section.

Chapter 3 "Grid-connected inverter as the integration block to the grid and AC loads". It is focused on grid connected inverters, which are the interface between multiple DC port converters and the AC grid. Therefore, if any of these multiple DC port converters must be connected to the grid, an inverter is required. The chapter is divided in 8 sections. The 1st section describes the inverter's main operation modes. The 2nd section reviews the modeling of the inverter which is the basis for advanced control methods. Based on that, the 3rd section proposes a methodology for designing the control blocks in a proportional multi-resonant scheme where the harmonics of the grid can be compensated. The 4th section, as a contribution, modifies that control method and makes it adaptive to grid changes. The 5th section is focused on methods based on the dq-frame. It models the inverter in dq-frame and particularly it is focused on the synchronization method and how the line impedance affects to the synchronization. The 6th section considers that the current control loop is performed and uses that control loops to make a voltage control loop, or in other words, a grid-forming inverter. It describes the model of the whole inverter including the high-level control blocks: virtual impedance, droop control and power filter. It provides simulation of a whole system with two connected inverters.

After that, the 7th section explains the limitations of the power sharing introduced in the previous section. It analyses the effect of the elements introduced previously and gives a guideline for parameter selection. In addition, the section introduces a new method for limiting the inverter's power, particularly in transients where, traditionally, the power sharing is not well controlled. Finally, the 8th section is focused on the reactive power sharing and proposes a communication between inverters using power-lines communication to adjust such power.

This inverter should be able to be flexible, because if it is delivering energy to the multiple active bridge, it mainly works as a rectifier, however if it provides energy to the grid, it will work as an inverter with limited current for protecting the EV battery.

In addition, those inverters connected to the grid should be able to provide grid services. For example, in case of grid failure, inverters from the EV chargers can take energy from the EV and give it to the grid to keep the grid stable for a short amount of time. For that, inverters should be able to work in different modes:

(a) Current-mode or slave mode, for absorbing or delivering a controlled amount of current (or power) from/to the grid according to a certain reference
(b) Voltage-mode or master mode, for delivering or absorbing as much power that the grid needs to keep the voltage stable.
(c) Multi-master mode or droop-mode, similar to the previous one but the inverters can work in parallel with the grid without any communication link. This is extremely useful in case of faults so inverters can share the power of a microgrid.
(d) DC voltage control mode, in this mode the inverter works as a rectifier following a DC voltage reference. This is the mode for the EV charging.

All of these different modes of control of inverters have some basic elements inside. The first one is the synchronization unit. There are many methods for synchronization, one of the most popular is based on a phase-locked loop (PLL). A PLL tracks the phase of a signal, for grid applications, the grid phase. Using Park and Clarke transformations, the grid voltage can be transformed in a phasor: $\overline{V(t)}e^{j\varphi(t)}$. A phasor is a complex number with a complex exponential which is rotating the phase [A5]. Based on those transformations, two components of the complex number can be obtained. Then, considering that the grid voltage should be in the real axis (in-phase axis, d), the quadrature voltage (in the q-axis) is proportional to the phase difference between the PLL generated phase and the grid phase [A4]. Thus, using a controller with two integrators the phase error can be zero although the signal is growing constantly φ=ωt. Therefore, a PLL which includes a PI and an extra integrator is used. On top of that, notch-filters can be used to minimize negative sequence signals in non-balance three-phase systems. In this work, two PLL where used to make sure that the phase difference of the inverter never reaches a critical value. One of the PLL block is used to create a phase limiter, which limits the power transfer [A4, A16, A18].

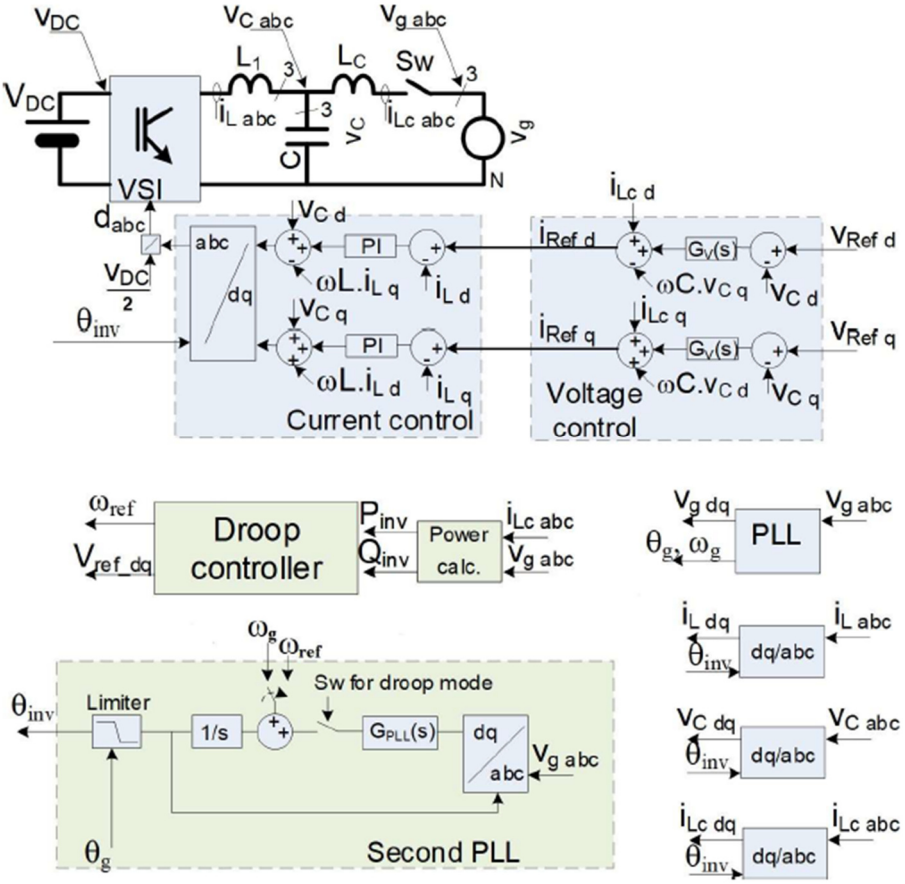

Figure 14- Complete block diagram of the proposed solution

Once, the PLL is tuned and is able to track the grid, the converter can work in the synchronous frame, considering that the grid voltage is $\overline{V(t)}e^{j\varphi(t)}.e^{-j\varphi_{PLL}(t)} = V_d$. This means that the converter control loops are "rotating" with the grid phase. In other words, the signals that the inverter control loops see are "DC type" signals ($V_d(t)$), not AC signals. They are not sinusoidal but variable DC signals related to the amplitude of

the AC signal. There are two signals that can be extracted from each converted signals, the in-phase (with the V_d) signal and the quadrature signal. As an example, if the three-phase currents are measured and transformed using Clarke and Park transformation with the phase obtained from the PLL unit, then the results are in-phase current and in-quadrature currents respect to the grid voltage ($i_d(t)$, and $i_q(t)$). The full diagram of a modified inverter control is shown in Figure 14.

By controlling only the current in the inverter using a reference, (a) the current-mode or slave mode inverter is defined. This inverter can absorb or deliver any amount of active or reactive power according to its reference. This is the typical inverter in solar generation where a maximum power point unit is dictating which is the current reference in the inverter. Notice that this control method is focused only on the phasor that rotates with the grid frequency but it does not control any other current at different frequencies. If harmonics need to be minimized, multi-resonant techniques can be applied [A15, A19]. In this research work, a scheme based on multi-resonant converters is proposed for harmonic reduction, the controller adapts its coefficients according to the harmonic amplitude levels.

By means of the current control loop, the inverter can control the currents to control further variables such as output voltage [A21]. Thus, a secondary control loop, the voltage control loop, excites the current (inner) control loop adjusting the current references to keep the output voltage to the desired level. This is the (b) voltage-mode or master mode inverter. It is used when the inverters work connected to an energy storage source, such as a battery. The inverter gives as much as current as the load needs in order to regulate the output voltage. It is call master mode because, in a grid, one inverter must control the voltage so other inverters can inject or absorb current, which are the slave-mode or current-controlled inverters.

This mode is useful but for massive grids, it is not convenient that only one inverter is controlling the voltage. Thus, a (c) multi-master mode or droop-mode is required. For that, an extra control block is required, the droop control unit [A19, A21, A22]. This unit reduces the phase of the inverter as a function of the “efforts” or its delivered active power. Thus, the inverter which is delivering more power tends to reduce its phase angle, and by reducing it, the delivered power also is reduced and this leaves a place for other inverters to give more power. Finally, this reaches an equilibrium, a power balance. The dynamic of the process can be controlled. In this work, several approaches to minimize the active and reactive power oscillations are presented based on power filters, virtual impedance techniques and communication through power lines [A1, A4, A16, A18, A20]. Using this droop control unit, inverters can share the load by delivering, each of them, a fraction of the active and reactive power. This is extremely useful in grids where the power delivered by a single inverter is not enough.

Finally, current-controlled inverters can also absorb power by selecting negative references, thus, the power is transferred from its AC side to its DC side. On top of the current control loop, a secondary control which measures the DC side and keeps it constant is useful in applications where the energy should be transfer from AC to DC. Such applications are electric vehicles, un-interruptible power supplies and others. In

the proposed EV charger, this is the (d) DC voltage control mode. This mode is required to charge the battery while the other modes are used for extracting energy from the vehicle to the grid (V2G mode). All of this modes are used in the proposed EV charger.

Chapter 4 "Partially isolated converters: Alternative topologies for multi-port system". This chapter suggests new topologies for multiple port converters in the case that not all of the ports require galvanic isolation. It includes four sections. The 1st section proposed a new hard-switching compact non-isolated topology. The 2nd section describes a new technique for bidirectional resonant converters in discontinuous current mode. The 3rd section extends this, to the continuous current mode. Finally, the 4th section, uses the concepts of the previous sections to propose a resonant multiple port converter with an AC port and one non-isolated DC port and one isolated DC port. Figure 1(c) shows that a non-isolated multiport converter and an isolated inverter can be used as an alternative to Figure 1(b). A non-isolated converter can be as simple as a combination of half-bridge converters, however, usually sources and loads have very different voltages and so a "high-gain" conversion is needed [A6, A24]. A conversion of more than 4 times is considered as high gain due to the limitation of performing in a single basic step-up (boost) converter. Thus, in this thesis a new circuit is proposed and shown in Figure 15. The static and the small-signal model is presented in the thesis including the control design, numerical simulation and experimental validation. This converter can be connected as in Figure 1(c) to an isolated inverter to provide multiple non-isolated DC ports in one side of the insulation while the AC port is in the other side.

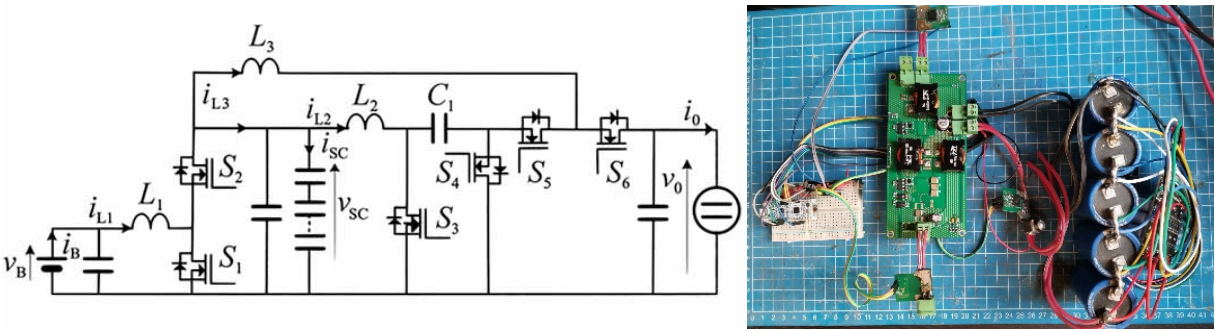

Figure 15- High-gain non-isolated converter: (a) main circuit, (b) prototype

A better approach can be done as Figure 1(d) shows, by means of a resonant DC/AC converter [A7]. Resonant converters with a special boosting technique can be used as bidirectional DC/DC converters for energy storage applications [A8-A14]. The boost technique produces a short circuit during a time-interval charging a resonant inductor. After that, the energy is released in a resonant capacitor which increases the output voltage of the converter. This is the main mechanism to work in a bidirectional mode in series resonant converter. The model of this technique, numerical simulations and experiments are detailed in this dissertation.

Using this DC/DC resonant boosting technique, an DC/AC (inverter) can be also obtained by means of overmodulation. The overmodulation consists of adding an additional pattern at a different frequency and by means of frequency division using filters, different power flow can be conducted. In resonant converters, the energy flows

at a certain frequency (close to the resonant frequency of the converter) thus a high-frequency isolation transformer can be used. The overmodulation adjusts the duty cycle of the converter with an external signal, as an example the voltage in the n-th port changes can be represented as, using Fourier series:

$$v_n(t) = \sum_{k=1}^{\infty} \frac{4}{\pi k} V_{DCn} . \sin(D_{nk}\pi + d(t)\pi) \sin(\omega_k t + \varphi_{kn}) \quad (35)$$

where the external signal is

$$d(t) = A \sin(\omega_{50Hz} t + \varphi_{50Hz})$$

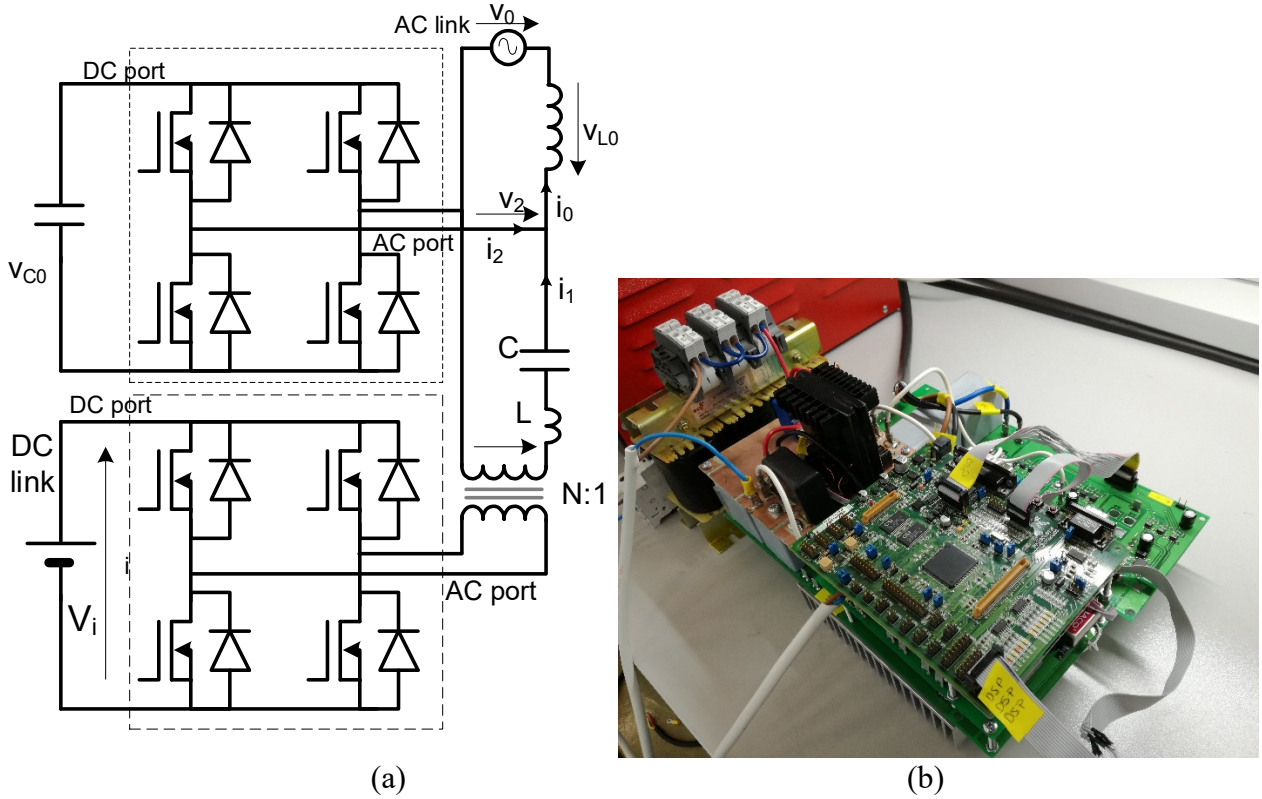

(a) (b)

Figure 16- Partial isolated DC//DC/AC inverter. One DC port fully isolated and one DC port with one AC port interconnected: (a) main circuit, (b) prototype

Using overmodulation, the converter will work simultaneously with several frequencies. For example, the grid and switching frequencies, the low frequency (50Hz) signal can be extracted with a low-pass filter. Therefore, this technique can allow: one isolated DC port and an DC port connected to an AC port as Figure 16 shows. The details of achieving this complex modulation is presented in the full dissertation including the modeling, numerical simulation and validation through experimental results.

CONCLUSIONS

The research work explains in detail the current state of the art of the elements in an EV charger, and proposes several contributions to increase its features in terms of new functions, smaller size and higher efficiency. The work focuses on the development of new control techniques and new circuit topologies that allow multiple port systems such as EV chargers to work efficiently in terms of low power losses with

ease of extending to large number of ports and implementation in real hardware based on industrial microprocessors. The dissertation has three main parts: multiple port converters, advanced modeling and control for inverters and partially isolated converters. The main contributions of each part are summarized below.

Multiple port converters: Based on Multiple Active Bridge (MAB) converter topology, a new modeling inspired on grid-tied inverters was developed in order to create a new control method which allows MAB converters to have a variable range of DC voltage in each port. The results are new possibilities for using that circuit to connect directly to batteries, supercapacitors, PV panels and other DC sources. The results show that a high-efficient multiple port converter can be used in many applications such as EV chargers, smart houses, multi-source/multi-load systems, hybrid energy storage systems and many others.

It is worth mentioning that, in comparison to other solutions for multi-port systems, such as a set of two-port converters, this research work opens new possibilities for the use of multiple active bridge converter. The impact of this work is on the cost and size of the multi-port system in terms of reducing the number of components and efficiency increase. In comparison with other control methods using the same topology, it was clarified in the research work that the modulations and control technique was oriented to variable DC ports and, in that condition, the proposal has a better efficiency.

Particularly, the results show a validation of a new mathematical model for describing the multiple active bridge based on dq-frame working at high-frequencies, at the switching frequency of the converter. Using that model, a decoupling control method that allows the use of any number of ports in a multiple active bridge converter and allows transferring energy from any port to any other port without sending power to any third port was proposed. The method also allows controlling the reactive power in the converter for the first time. With this new degree of freedom, soft-switching techniques can be implemented to reduce the power losses. In addition, the control method compensates the effect of the voltage change in the DC ports which results in a higher converter's efficiency in comparison with other control methods (single phase shift method) in the condition of non-equal voltage at the DC ports. As an additional novelty, a specific modulation called "dual duty" was proposed and implemented in order to reduce conduction losses and increase efficiency for power delivery. The aim of this modulation technique is to minimize the root mean square current through the transformer's windings.

Advanced modeling and control for inverters. Emphasis was put on improving the active and reactive power sharing in the grid using inverters. In the future, EV chargers should be able to absorb energy from the grid (charging the EV battery) but also provide services to the grid by delivering energy (vehicle-to-grid, V2G mode). For that, inverters can be used in multi-master mode, connected to the grid and control the voltage in their nodes but also accept power from other nodes in a power-sharing fashion. This thesis introduces new elements for improving transients and reducing power oscillations when inverters are connected to the grid as masters or grid-forming inverters. Concretely, the results are a reduction in power oscillations during connection transients by means of power filters, virtual impedance and the introduction

of a phase limiter. The phase limiter is a new method to control and limit the output power of inverters during transients. Moreover, the controller of the inverter should tolerate changes in the grid, thus, an adaptive controller was proposed which controls the output current of the inverter and compensated the possible harmonics.

Partially isolated multi-port converters. The previous solution guarantees that all ports have galvanic isolation which increases the safety of the system. However, it might not be required that all of the ports have this feature but only some of them. Then, two main alternatives can be used: non-isolated converters with isolated inverter, which can give a partial isolated solution for EV chargers, however, isolated inverters are bulky. This dissertation introduces a better solution based on resonant inverters. This resonant multi-port converter is a more compact alternative, but has a limited number of isolated ports. The proposed solution is based on resonant power flow and an overmodulation which allow an AC grid-frequency power flow and a resonant power flow through high frequency transformers to provide isolation.

The proposed resonant partial isolated converter is promising due to the compactness of the solution. However, this circuit is still in an early stage due to its limited efficiency. This makes the MAB converter combined with the inverter a more viable industrial solution. The main drawback of the resonant converter is its efficiency transferring energy from AC to isolated DC due to the hard-switching technique in the AC/DC conversion process. Advanced semiconductors and soft-switching techniques can be applied to improve the converter's efficiency and make it more competitive.

Future work involves the combination of MAB control techniques with the proposed resonant techniques in order to have the benefits of both approaches. In general, all of the topics can be implements in the power electronic industry in the close future because they do not require any special element, thus, the proposed benefits can be included in future products

BIBLIOGRAPHY:

1. Lu. J. Multimode Operation for On-Line Uninterruptible Power Supply System / J. Lu., M. Savaghebi, S. Golestan, J. C. Vasquez, J. M. Guerrero, A. Marzabal // IEEE J. Emerg. Sel. Top. Power Electr. – 2019 - Vol. 7 No.2. – P. 1181–1196
2. Wu F. TAB Series-Resonant DC-DC Converter and Multi-Phase-Shift Based Global Optimization Modulation/ F. Wu, K. Wang, J. Su // Appl. Sci. (Basel) – 2022. - Vol. 12 No. 13. - P. 67-83
3. Oluwasogo E.S. Self-Current Sharing in Dual-Transformer-Based Triple-Port Active Bridge DC–DC Converter With Reduced Device Count / E. S. Oluwasogo, H. Cha // IEEE Trans. Power Electron. – 2021 - Vol. 36 No. 5 - P. 5290–5301
4. Zhang X. Research on Power Decoupling and Parameter Mismatch of Three-Port Isolated Resonant DC-DC Converter Applied Switch Controlled Capacitor / X. Zhang, H. Liu, P. Wheeler, F. Wu // IEEE Trans. Ind. Electron. – 2023 - Vol. 70 No. 8 - P. 8098–8107
5. Pereira T. Self-Tuning Multiport Resonant DC/DC Converter Based on Actively-Controlled Inductors for Hybrid Storage System Integration / T.

Pereira, Y. Wei, Y. Pascal, H. A. Mantooth, M. Liserre // IEEE, Transl. Power Electron – 2022 - Vol. 38 No. 4 - P. 4787-4804.

6. Cao L. An Immittance-Network-Based Multiport ZVS Bidirectional Converter With Power Decoupling Capability / L. Cao, J. Lin, X. Jiang, C. S. Wong, K. Loo // IEEE Trans. Power Electron – 2022 - Vol. 37 No. 10 – P.12729–12740
7. Zhao C. An isolated three-port bidirectional dc-dc converter with decoupled power flow management / C. Zhao, S. D. Round, J. W. Kolar // IEEE Trans. Power Electron. – 2008 - Vol. 23 No. 5 - P. 2443–2453
8. Koohi P. A survey on multi-active bridge dc-dc converters: Power flow decoupling techniques, applications, and challenges / P. Koohi, A. J. Watson, J. C. Clare, T. B. Soeiro, P. W. Wheeler // Energies – 2023 - Vol. 16 No. 16 - P. 5927
9. Shao S. Modeling and Advanced Control of Dual-Active-Bridge DC–DC Converters: A Review / S. Shao, L. Chen, Z. Shan, F. Gao, H. Chen, D. Sha, T. Dragičević // IEEE Trans. Power Electron – 2022 - Vol. 37 No. 2 - P. 1524–1547
10. Ibanez F. M. An Impedance Based Modeling Towards the Aging Prediction of Lithium-Ion Battery for EV Applications / Ibanez, T. Ahmed, I. Idrisov, J. S. Gutierrez – Proc. of 8th International Conference on Renewable Energy Research and Applications (ICRERA) – IEEE, 2019
11. Ibanez F. M. Design Balancing Systems for Supercapacitors Based on Their Stochastic Model / F. M. Ibanez, I. Idrisov, F. Martin, A. Rujas // IEEE Trans. Energ. Convers. – 2020 - Vol. 35 No. 2 - P. 733–745
12. Zhao, C. A novel three-phase three-port UPS employing a single high-frequency isolation transformer / C. Zhao, J.W. Kolar // Proc. of IEEE 35th Annual Power Electronics Specialists Conference (APEC'04) – IEEE - 2004
13. Wang, L. Asymmetrical duty cycle control and decoupled power flow design of a three-port bidirectional DC-DC converter for fuel cell vehicle application / L. Wang, Z. Wang, H. Li // IEEE Trans. Power Electron. – 2012 – Vol. 27 No. 2 – P. 891–904
14. Duarte, J.L. Three-port bidirectional converter for hybrid fuel cell systems. / J. L. Duarte, M. Hendrix, M. G. Simoes // IEEE Trans. Power Electron. – 2007 – Vol. 22 No 2 – P. 480–487
15. Neubert, M. Performance analysis of a triple-active bridge converter for interconnection of future dc-grids / M. Neubert, A. Gorodnichev, J. Gottschlich, R.W. De Doncker // Proc. of IEEE Energy Conversion Congress and Exposition (ECCE'16) – IEEE, 2016
16. Falcones, S. A DC–DC multiport-converter-based solid-state transformer integrating distributed generation and storage / Falcones, S., Ayyanar, R., Mao, X. // IEEE Trans. Power Electron – 2013 – Vol. 28 No. 5 – P. 2192–2203
17. Costa, L.F. Optimum design of a multiple-active-bridge DC–DC converter for smart transformer / L.F. Costa, G. Buticchi, M. Liserre // IEEE Trans. Power Electron. Vol. 33 No. 12 – P. 10112–10121
18. Karanayil B. Power flow management of isolated multiport converter for more electric aircraft / B. Karanayil, M. Ciobotaru, V.G. Agelidis // IEEE Trans. Power Electron – 2017 – Vol. 32 No. 7 – P. 5850–5861

19. N.D. Dao. High-efficiency SiC-based isolated three-port DC/DC converters for hybrid charging stations / Dao, N.D., Lee, D., Phan, Q.D. // IEEE Trans. Power Electron. – 2020 - Vol 35 No 10, P. 10455–10465
20. Rashidi, M. Design and development of a high-frequency multiport solid-state transformer with decoupled control scheme / M. Rashidi, N.N. Altin, S.S. Ozdemir, A. Bani-Ahmed, A. Nasiri // IEEE Trans. Ind. Appl. – 2019 – Vol.55 No 6, P. 7515–7526
21. Hebala, O.M. Generalized active power flow controller for multiactive bridge DC–DC converters with minimum-current-point-tracking algorithm / O.M. Hebala, A.A. Aboushady, K.H. Ahmed, I. Abdelsalam // IEEE Trans. Ind. Electron. – 2022 – Vol. 69 No.4 – P. 3764–3775
22. Vermulst, B.J. Scalable multi-port active-bridge converters: Modelling and optimised control / B.J. Vermulst, J.L Duarte, E.A. Lomonova, K.G. Wijnands // IET Power Electron – 2017 - Vol. 10, P. 80–91
23. Yazdani A. Voltage-Sourced Converters in Power Systems: Modeling, Control, and Applications / A. Yazdani, R. Iravani - Wiley-IEEE Press, 2010
24. Bin W. Current-Source Converter and Cycloconverter Topologies for Industrial Medium-Voltage Drives / W. Bin, J. Pontt, J. Rodriguez, S. Bernet, S. Kouro // IEEE Transactions on Ind. Electronics – 2008 – Vol. 55 No.7 – P. 2786–2797
25. Gupta K. K. Multilevel Inverter Topologies With Reduced Device Count: A Review / K. K. Gupta, A. Ranjan, P. Bhatnagar, L. K. Sahu, S. Jain // IEEE Transactions on Power Electron – 2016 - Vol. 31 No. 1 – P. 135-151
26. Bandyopadhyay S. Control of Multiactive Bridge Converters Using Linear Active Disturbance Rejection / S. Bandyopadhyay, Z. Qin, P. Bauer // IEEE Trans. Ind. Electron. – 2021 – Vol. 61 No. 11 – P. 10688–10698
27. Cai Y. A Modular Modulation Decoupling Algorithm for Multiple Active Bridge Based Multiport EV Charger / Y. Cai, J. Li, C. Gu, J. Yang, S. Guenter, G. Buticchi, et al. // IEEE J. Emerg. Sel. Top. Power Electron. – 2024 – Vol. 12 No4 – P. 3637–3649
28. Liu Q. Review and Comparison of Grid-Tied Inverter Controllers in Microgrids / Q. Liu, T. Caldognetto and S. Buso // IEEE Transactions on Power Electronics – 2020 – Vol. 35 No 7 – P. 7624-7639
29. Kumar Barik P. A novel negative feedback phase locked loop-based reference current generation technique for shunt active power filter / P. Kumar Barik, G. Shankar, P. Kumar Sahoo, R. Madurai Elavarasan, Sachin Kumar, F. M. Ibanez, M. Abou Houran, Ankit Kumar Srivastava, Vladimir Terzija // International Journal of Electrical Power & Energy Systems – 2023 – Vol. 153 – P. 109389
30. Meng X. A Generalized Droop Control for Grid-Supporting Inverter Based on Comparison Between Traditional Droop Control and Virtual Synchronous Generator Control / X. Meng, J. Liu, Z. Liu // IEEE Trans Power Electron. – 2019 – Vol. 34 No.6 – P. 5416–5438
31. Kazimierczuk M.K. Resonant power converters / Kazimierczuk M.K. Czarkowski D - Wiley-Interscience, 1995

PUBLICATIONS OF THE AUTHOR ON THE SUBJECT OF THE DISSERTATION

A1. AlSadat M. Using low bandwidth communication through power lines to enhance reactive power sharing for inverters-based microgrids / M. AlSadat, F.M. Ibanez, I. Elghanam, V. Terzija // International Journal of Electrical Power & Energy Systems – 2024 – Vol. 159 – P. 110043

A2. Ibanez, F.M. Control method based on real–imaginary decomposition at the switching frequency for multiple active bridge converters / F.M. Ibanez, A. Shubnaya, F. Martin // IET Power Electron – 2024 – Vol. 17 – P. 1287–1300..

A3. A. Shubnaya. Minimizing conduction losses in multiple active bridge converters across wide voltage ranges using advanced dual-duty modulation / A. Shubnaya, M. Koksharov, F. Martin, A. Galarza, F.M. Ibanez // IET Power Electron. – 2024 – Vol 17 – P. 2698–2713.

A4. Ibanez F.M. Improving the power sharing transients in droop-controlled inverters with the introduction of an angle difference limiter / F.M. Ibanez, M. AlSadat, Y. Vlasov, V. Peric, P. Vorobev // International Journal of Electrical Power & Energy Systems – 2023 – Vol. 153 – P. 109371.

A5. P.K. Barik. A novel negative feedback phase locked loop-based reference current generation technique for shunt active power filter / Barik PK, Shankar G, Sahoo P.K., Elavarasan RM, Kumar S, Ibanez F.M., Houran M. A., Srivastava A. K., Terzija V. // International Journal of Electrical Power & Energy Systems – 2023 – Vol. 153 – P. 109389.

A6. Davalos Hernandez F. A Dual-Input High-Gain Bidirectional DC/DC Converter for Hybrid Energy Storage Systems in DC Grid Applications / F. Davalos Hernandez, R. Samanbakhsh, P. Mohammadi, F.M. Ibanez // IEEE Access – 2021 - Vol. 9 – P. 164006-164016.

A7. Ibanez F.M. Bidirectional Series Resonant DC/AC Converter for Energy Storage Systems / F.M. Ibanez // IEEE Transactions on Power Electronics – 2019 - Vol. 34 No. 4 – P. 3429-3444.

A8. Florez-Tapia AM. Small signal modeling and transient analysis of a Trans quasi-Z-source inverter / AM Florez-Tapia, FM Ibanez, J Vadillo, I Elosegui, J.M. Echeverria // Electric Power Systems Research – 2017 – Vol. 144 – P. 52-62.

A9. Ibanez F.M., State-Plane Analysis of Anomalous Step-Up Behavior in Series-Resonant Converters / F.M. Ibanez, J.M. Echeverria, J. Vadillo, L. Fontan // IEEE Journal of Emerging and Selected Topics in Power Electronics – 2016 – Vol 4. No 3 – P. 1026-1035.

A10. Ibanez, F.M. Multimode step-up bidirectional series resonant DC/DC converter using continuous current mode / F.M. Ibanez, J.M. Echeverria, D. Astigarraga, L. Fontan // IET Power Electronics – 2016 – Vol. 9 – P. 710-718.

A11. Ibanez F.M. A Step-Up Bidirectional Series Resonant DC/DC Converter Using a Continuous Current Mode / F.M. Ibanez, J.M. Echeverria, J. Vadillo, L. Fontan // IEEE Trans. on Power Electronics – 2015 - Vol. 30 No. 3 – P. 1393-1402.

A12. Ibanez F. M. High-Current Rectifier Topology Applied to a 4-kW Bidirectional DC–DC Converter / F. Ibanez, J. M. Echeverria, J. Vadillo L.

Fontan // IEEE Transactions on Industry Applications – 2014 – Vol. 50(1) – P. 68-77.

A13. Ibanez, F.M. Frequency response analysis for bidirectional series-resonant DC/DC converter in discontinuous mode / F. M. Ibanez, J.M. Echeverria, J. Vadillo, L. Fontan // IET Power Electronics – 2014 – Vol. 7 – P. 2374-2386.

A14. F. M. Ibanez. Novel technique for bidirectional series-resonant DC/DC converter in discontinuous mode / F.M. Ibanez, J.M. Echeverria, L. Fontan // IET Power Electronics – 2013 – Vol. 6. – P. 1019-1028.

A15. Veretennikov I. Proportional Multiresonant Controller with Automatic Gains Adjustment for Grid-Connected Inverters / I. Veretennikov, Y. Vlasov, F.M. Ibanez, V. Terzija, A.A. Nazeri // Proc. IEEE Belgrade PowerTech - 2023 - P. 1-6. DOI: 10.1109/PowerTech55446.2023.10202847

A16. AlSadat M. Improving Transients for Droop-Controlled Inverters / M. AlSadat, Y. Vlasov, P. Vorobev, V. Terzjia, F. Ibanez, V.S. Perić // Proc. IEEE Appl. Power Electron. Conf. Expo. (APEC) – 2023 - P. 1-6. DOI: 10.1109/APEC43580.2023.10131238.

A17. Shubnaya A. Compensating measurement delays in decoupling blocks of dq control technique for multiple active bridge converter / A. Shubnaya, F.M. Ibanez, P. Rodriguez Cortes // Proc. 48th Annu. Conf. IEEE Ind. Electron. Soc. (IECON) - 2022 - P. 1-6. DOI: 10.1109/IECON49645.2022.9968549.

A18. Ibanez F.M. Limiting transients for grid-forming inverters using a phase limiter / F.M. Ibanez, M. AlSadat, Y. Vlasov, P. Vorobev, V. Terzija, P. Pant, V. Peric // Proc. of 11th International Conference on Renewable Energy Research and Application (ICRERA) – IEEE – 2022 - P. 1–6. DOI: 10.1109/ICRERA55966.2022.9922712.

A19. Nazeri A.A. Paralleled Modified Droop-Based Voltage Source Inverter for 100% Inverter-Based Microgrids / A.A. Nazeri, P. Zacharias, F.M. Ibanez, I. Idrisov // Proc. IEEE Ind. Applic. Soc. Annu. Meeting (IAS) – 2021 - P. 1-6. DOI: 10.1109/IAS48185.2021.9677365.

A20. AlSadat M. Reactive Power Sharing Utilizing Low Bandwidth Communication Through Power Lines / M. AlSadat, F.M. Ibanez // Proc. IEEE Power Energy Soc. Gen. Meet. (PESGM) – 2021 - P. 1-5. DOI: 10.1109/PESGM46819.2021.9638164.

A21. Nazeri A.A. Design of Proportional-Resonant Controller with Zero Steady-State Error for a Single-Phase Grid-Connected Voltage Source Inverter with an LCL Output Filter / A.A. Nazeri, P. Zacharias, F.M. Ibanez, S. Somkun // Proc. IEEE Milan PowerTech - 2019 - P. 1-6. DOI: 10.1109/PTC.2019.8810649.

A22. Majidi M. A guideline for modeling voltage and frequency controls in ac microgrids: The influence of line impedance on transient time / M. Majidi, A.A. Nazeri, F.M. Ibanez, D. Pozo // Proc. IEEE Milan PowerTech – 2019 - P. 1-6. DOI: 10.1109/PTC.2019.8810772.

A23. Mohammadi P. High Frequency Transformer Design for Specific Static Magnetising and Leakage Inductances Using Combination of Multi-Layer Perceptron Neural Networks and FEM Simulations / P. Mohammadi, R.

Samanbakhsh, P. Koohi, F. Ibanez // Proc. of IEEE 10th International Symposium on Power Electronics for Distributed Generation Systems (PEDG), IEEE – 2019 – P. 1–6. DOI: 10.1109/PEDG.2019.8807556.

A24. Mohammadi P. A Novel Non-Coupled Non-Isolated Double-Input Bidirectional High-Gain Converter for Hybrid Energy Storage System / P. Mohammadi, R. Samanbakhsh, F.D. Hernandez, P. Koohi, F.M. Ibanez // Proc. IEEE 10th Int. Symp. Power Electron. Distrib. Gener. Syst. (PEDG) – 2019 - P. 1-6. DOI: 10.1109/PEDG.2019.8807556.

A25. Ibanez F.M. Anomalous step-up behavior in discontinuous series resonant converters / F.M. Ibanez, J. Vadillo, J.M. Echeverria, L. Fontan // Proc. IEEE Workshop Control Model. Power Electron. (COMPEL) - 2014 - P. 1-6. DOI: 10.1109/COMPEL.2014.6877129

A26. Ibanez F. M. 100kW bidirectional DC/DC converter for a supercapacitor stack / F. M. Ibanez, J. Vadillo, J. M. Echeverria L. Fontán // IEEE PES ISGT Europe – 2013 - P. 1-5. DOI: 10.1109/ISGTEurope.2013.6695246.

A27. Ibanez F. M. 25kW DC/DC Converter applied to a supercapacitor stack / /F. M. Ibanez, J. M. Echeverria, J. Vadillo and L. Fontán // Proc. 2012 Electrical Systems for Aircraft, Railway and Ship Propulsion – 2012 – P. 1-6. DOI: 10.1109/ESARS.2012.6387429.

A28. Патент No 2831526 Российская Федерация, СПК H02J 7/00 (2024.08). ЗАРЯДНОЕ УСТРОЙСТВО ДЛЯ ЭЛЕКТРОМОБИЛЕЙ С НЕСКОЛЬКИМИ ИСТОЧНИКАМИ ЭНЕРГИИ: No 2024122493: заявлено 06.08.2022:
опубликовано: 09.12.2024 / Ибаниес Федерико Мартин, Власов Ярослав, Сергеевич, Веретенников Илья Олегович, Идрисов Ильдар Наилевич, Афонин Михаил, Михайлович.; заявитель и патентообладатель Сколковский институт науки и технологий. – 14 с.